INTRA-SWASH HYDRODYNAMICS AND SEDIMENT FLUX FOR DAMBREAK SWASH ON COARSE-GRAINED BEACHES

T. O'Donoghue[1*], G. A. Kikkert[2], D. Pokrajac[1], N. Dodd[3] and R. Briganti[3]

[*] Corresponding author

[1]School of Engineering, University of Aberdeen, King's College, Aberdeen, United Kingdom, AB24 3UE (t.odonoghue@abdn.ac.uk; d.pokrajac@abdn.ac.uk)

[2]Department of Civil and Environmental Engineering, Hong Kong University of Science and Technology, Hong Kong (kikkert@ust.hk)

[3]Department of Civil Engineering, University of Nottingham, University Park, Nottingham, United Kingdom, NG7 2RD (Nicholas.Dodd@nottingham.ac.uk; Riccardo.Briganti@nottingham.ac.uk)

ABSTRACT

The paper reports on dambreak-type swash experiments in which intra-swash hydrodynamics and sediment flux are measured for swash on a coarse sand beach and a gravel beach. Flow velocity and depth are measured using PIV and LIF respectively; the intra-swash sediment flux is measured using sediment traps. Comparison of measured hydrodynamics with the immobile, permeable bed experiments of Kikkert et al. (2013) indicate that bed mobility impacts on the swash hydrodynamics, reducing the maximum run-up by approximately 8% for both beaches, compared to the maximum run-up on the corresponding immobile beach. The measured intra swash sediment flux at a given location is characterised by high flux at the moment of bore arrival, followed by rapid decay during uprush, becoming zero at some time before flow reversal. For the gravel beach, the backwash sediment flux is negligibly small, while for the sand beach the backwash flux increases slowly as the flow accelerates down the beach, and peaks at about the time of maximum backwash velocity. Intra-swash sediment flux calculated using the Meyer-Peter and Müller bed load transport formula, with measured hydrodynamics as input and bed shear stress estimated using both the Swart and Colebrook formulae, are within a factor 2 of the measured intra-swash flux. The agreement between the calculated and measured flux is better for the sand beach than for the gravel beach, and better for uprush than for backwash. For the sand beach there is good agreement between calculated and measured total uprush and total backwash sediment volumes. The agreement is less good for the gravel beach, for which calculated and measured uprush volumes show a similar trend but the calculated backwash volumes over-estimate the (negligible) volumes observed in the experiments.

Keywords swash, hydrodynamics, sediment transport, shear stress, laboratory, dam-break

1.0 INTRODUCTION

Swash on steep, coarse-grained beaches is generated by the collapse of wave bores on the beach slope, resulting in high flow velocities with potential for substantial sediment flux and morphological change. Hydrodynamics and sediment dynamics within a swash event are complex because of the highly turbulent and aerated nature of the collapsing bore and the high unsteadiness and non-uniformity of the flow across the swash zone. In field conditions the complexity is augmented by interactions between swash events of varying magnitude and duration, caused by the varying period and amplitude of the incident waves, and by the effects of low-frequency water surface oscillations in the surf and swash zones.

Field experiments investigating swash hydrodynamics and sediment dynamics have developed substantially over the last two decades in terms of the sophistication of the instruments deployed and the degree to which detailed processes are captured by the measurements. Regarding sediment flux, sediment trapping has been used to measure total uprush and total backwash transport volumes (Hughes et al., 1997; Masselink and Hughes, 1998; Austin & Masselink, 2006; Masselink et al., 2009) and high-resolution bed elevation measurements across the swash zone have been used to obtain net sediment transport volumes for individual swash events (e.g. Blenkinsopp et al., 2011). These measurements are extremely valuable in terms of quantifying sediment fluxes and morphological change for swash events in the field. However, they do not provide a complete picture since they reveal little (in the case of traps) or nothing (in the case of bed elevation measurements) of the sediment flux during a swash event. In principle, measurements of intra-swash sediment flux can be obtained from co-located measurements of velocities and concentrations, but obtaining these measurements sufficiently accurately over the complete water column to give total sediment flux through the full swash cycle remains a significant practical challenge (Blenkinsopp et al., 2011).

In the laboratory, small-scale wave flumes have been used to study swash hydrodynamics over immobile, impermeable beaches (e.g. Petti and Longo, 2001; Cowen et al., 2003; Gedik et al., 2005; Shin and Cox, 2006; Sou et al., 2010; Rivillas-Ospina et al., 2012). Large-scale wave flume experiments have studied sand suspension processes in the swash zone (Alsina and Caceres, 2011; Caceres and Alsina, 2012), interactions between surf and swash bed dynamics (Alsina et al., 2012), the effects of

long waves, wave groups and random waves on surf and swash bed dynamics (Baldock et al., 2011) and beach groundwater effects on swash sediment transport (Masselink and Turner, 2012). These have yielded insights into swash zone sediment processes and morphology, but, as for field experiments, estimates of swash sediment transport are either inferred from bed elevation measurements or are limited to suspended sediment flux based on co-located velocity and suspended sediment concentration measurements. More recently, van der Zanden et al. (2015) and Puleo et al. (in press) obtained measurements of intra-swash sediment concentrations and velocities within the sheet-flow layer of swash in large-scale wave flume experiments. The studies used conductivity-based instrumentation for the concentration measurements; for the sheet-flow velocities, Puleo et al. (in press) used an acoustic velocity profiler while van der Zanden et al. (2015) cross-correlated concentration measurements from a pair of concentration probes horizontally separated by 15 mm. Neither method was successful in fully resolving the velocities through the sheet-flow layer and through the whole swash cycle. Nevertheless, Puleo et al. (in press) combines their sheet-flow results with concentration and velocity measurements above the sheet-flow layer to estimate the relative contributions of suspended load and sheet-flow load to the total transport.

The complexity of processes at work in the field and in large-scale wave flume experiments makes it difficult to isolate and quantify fundamental processes and to provide measurements of the kind needed for the development of swash numerical models. An alternative to wave flumes for laboratory swash experiments is to generate swash via a dambreak, whereby a reservoir of water is suddenly released in a flume, leading to a bore that collapses on a beach located downstream. The dambreak produces a single, highly repeatable, large-scale swash event, with bore depth, bore speed and maximum run-up comparable to that seen in the field under energetic wave conditions. The set-up avoids many of the complexities associated with swash in the field, and indeed with wave-generated swash in laboratory wave flumes, such as the variability in swash events, swash-swash interactions and the effects of low-frequency oscillations. This reduction in complexity, combined with the ability to repeat the same swash event many times, allows particular fundamental swash processes to be isolated and studied in detail. Moreover, dambreak swash experiments provide good benchmark data for numerical models since the boundary and initial conditions are well defined and data are available with high resolution in time and space. Barnes et al. (2009) used a dambreak set-up to directly measure intra-swash bed shear stress using a shear plate; a similar set-up was used by O'Donoghue et al. (2010) and Kikkert et al. (2012) to study the detailed hydrodynamics of swash over immobile, impermeable beaches of varying surface roughness, and by Kikkert et al. (2013) and Steenhauer et al. (2011) to measure hydrodynamics over and within immobile, permeable beaches. The present study

uses the same dambreak facility as used for these previous experiments, but with the beach now consisting of mobile sediment, the primary objective being to measure the intra-swash sediment flux for well-controlled swash conditions. Previous dambreak swash experiments involving a mobile sediment beach are limited to Othman et al. (2014), who used a sloping dambreak apparatus to measure swash uprush sediment transport at the end of a truncated slope, their particular focus being on the influence of grain size and pressure gradient on sediment transport, not on the detailed intra-swash sediment flux.

This paper reports on dambreak swash experiments in which intra-swash flow depth, flow velocity and sediment flux are measured at a number of cross-shore locations for swash on beaches consisting of mobile, coarse-grained sediment. The experiments involve two beach types: a coarse sand beach and a gravel beach. The experimental setup is the same as that used for the permeable, immobile beach experiments of Kikkert et al. (2013), which means that for each of the present mobile bed experiments, the incident bore, beach slope, beach material and beach permeability are the same as for the corresponding immobile beach experiment reported by Kikkert et al. (2013). Comparing hydrodynamic measurements from the present experiments with the hydrodynamic measurements from Kikkert et al. (2013) therefore enables the effects of bed mobility on the swash hydrodynamics to be isolated and quantified. More importantly, the present experiments yield measurements of intra-swash sediment flux for well-controlled, large-scale swash events. To the authors' knowledge, intra-swash flux measurements of this kind, combined with detailed depth and velocity measurements, have not been reported previously.

The details of the experimental setup are presented in Section 2. Section 3 presents the experimental results for shoreline motion, swash depths and depth-averaged velocities, including comparisons with results from the corresponding immobile bed experiments of Kikkert et al. (2012, 2013) in order to quantify the effects of bed mobility on the swash hydrodynamics. The measured intra-swash sediment flux is presented in Section 4, followed in Section 5 by a comparison of the measured flux with the flux calculated using a bed load sediment transport formula. Section 6 concludes the paper with a summary of the main results.

2.0 EXPERIMENTAL SET-UP AND MEASUREMENTS

2.1 Set-up and test conditions

The experiments were carried out using the same facility used by Kikkert et al. (2012, 2013). A reservoir was placed at one end of a 20 m-long, 0.9 m-high and 0.45 m-wide, glass-sided flume (Figure 1). The reservoir is fronted by a gate, which is rapidly lifted by a falling-weight mechanism to produce a dambreak-generated bore. The reservoir is 0.983 m long (inside dimension), 0.394 m wide and filled with water to a depth of 0.600 m; the water depth in front of the gate was set at 62 mm. A 1:10 beach was located downstream from the reservoir. The initial shoreline on the beach, corresponding to the intersection of the water surface with the top of the beach roughness, was 0.623 m from the toe of the beach and 4.82 m from the gate. The origin of the $x-z$ coordinate system is at the initial shoreline, with the x-axis parallel to the beach slope and positive shoreward, and the z-axis perpendicular to the slope. The gate is raised at time t = 0, resulting in a plunging wave, which produces a bore, approximately 0.25 m high propagating with approximate speed 2.0 m/s towards the beach. The bore collapses on the beach, producing a single, repeatable swash event, with velocity, depth and maximum run-up magnitudes similar to those of full-scale swash in the field.

Experiments were carried out on two beach types: a coarse sand (CS) beach with d_{50} = 1.3 mm and a gravel (GV) beach with d_{50} = 8.4 mm. Constant head permeameter tests (Steenhauer et al., 2012) established Forcheimer coefficients $a_k = 81.2$ s/m, $b_k = 3587$ s^2/m^2 for the CS beach and $a_k = 4.1$ s/m, $b_k = 383$ s^2/m^2 for the GV beach (here $I = a_k u_D + b_k u_D^2$, where I is hydraulic gradient and u_D is Darcy velocity); the sand is therefore an order of magnitude less permeable than the gravel. The sediments are the same as those used for the corresponding immobile, permeable beach experiments reported in Kikkert et al. (2013), for which the top layer of the sediment beach was made immobile using a dilute cement mix, without changing the permeability (Steenhauer et al, 2011). The permeability of each of the present CS and GV mobile beaches is therefore equal to the permeability of each of the corresponding immobile, permeable beaches reported in Kikkert et al. (2013).

The sediment occupied the full beach, i.e. from the surface of the 1:10 beach face to the floor of the flume. Lines corresponding to the required 1:10 beach slope were drawn on the glass sides of the flume and the beach surface was matched to these lines before each swash run. The 1:10 lines on the glass were approximately 1mm thick. Between runs the sediment bed was re-shaped by hand so that the top surface of the sediment bed was as close as possible to the top of the line, but never above or below; hence the variation in initial bed level between runs is estimated to be of the order of 1mm. No sediment was present on the horizontal bed of the flume between the gate and the beach, which means the incoming bore does not arrive at the shoreline already loaded with sediment. This feature of the experiment differs from swash in the field, where bore-advected sediment can make a

significant contribution to sediment flux on the beach (Alsina et al., 2011). The far (downstream) end of the beach was supported by a vertical sheet of 30 mm-thick marine plywood, drilled with several large-diameter holes and covered with 1 mm-diameter stainless steel mesh to allow the beach to drain. Each experiment started with the beach groundwater level equal to the water level in front of the reservoir (62 mm). This was achieved using a weir with 62 mm crest elevation placed approximately 0.5 m beyond the end of the beach (Figure 1). Between experiments the beach was re-levelled to its 1:10 slope and the beach was given time to fully drain to the 62 mm groundwater level. Drainage times for the CS and GV beaches were approximately 60 mins and 6 mins respectively.

2.2 Hydrodynamic measurements

Simultaneous measurements of velocity and depth were obtained at a number of cross-shore locations using the combined particle image velocimetry (PIV) and laser-induced fluorescence (LIF) system previously described by Kikkert et al. (2012). The water in the reservoir was seeded with neutrally-buoyant 20 µm titania particles for the PIV measurements and with fluorescent dye (concentration 0.1 mg/l) for the LIF measurements. The PIV/LIF measurements were made at five cross-shore locations on the beach. At each location the Nd-YAG laser sheet was introduced to the flow through a window in the flume floor and a highly-polished perspex tower extending from the flume floor to the beach surface (Figure 1; see also Kikkert et al., 2013). Each tower was 20 mm wide and 200 mm long (in the cross-shore direction); the top edge had a 1:10 slope to match the beach slope and the height was such that the tower was flush with the beach surface at the measurement position. Velocities were not measured at the moment of bore arrival because of air bubbles and because of high sediment load blocking the light sheet. Thereafter, the presence of individual sediment grains in the flow give rise to spurious velocity vectors that were removed by the post processing. During the experiments the tower on the lower part of the beach became slightly exposed because of slight erosion in its vicinity; scour at the other towers was negligible. No tower was completely covered by sediment at the end of a swash run because accretion levels at the tower locations was close to zero.

DANTEC Dynamic Studio v1.45 software controlled the PIV and LIF cameras, enabling synchronised PIV and LIF images to be recorded at a frequency of 13.5 Hz. The PIV-LIF measurements were triggered at the moment of gate release. For the CS beach, simultaneous velocity and depth measurements were obtained at five cross-shore locations: x = 0.072, 0.772, 1.567, 2.377 m and 3.177 m. Because swash depth decreases with increasing x, the PIV camera view area was smaller higher up the beach: 231 mm x 173 mm at x = 0.072 m, reducing to 114 mm x 86 mm at x = 3.177 m. The resulting

instantaneous velocity vector fields have spatial resolution between 2.5 mm (at x = 0.072 m) and 1 mm (at x = 3.177 m), with corresponding random errors between 14 mm/s and 7 mm/s. The LIF-measured flow depth has a random error between 0.3 and 0.1 mm. For the CS beach, the simultaneous velocity and depth measurements were repeated 10 times for each of the five measurement locations; more repeats were not possible because of the long time to drain the beach following each swash run.

For the GV beach, simultaneous velocity and depth measurements were obtained at three cross-shore locations: x = 0.072, 0.772 and 1.567 m; the lower maximum run-up on the gravel beach precluded measurements at higher x . The PIV camera view area ranged from 241 mm x 181 mm at x = 0.072 m to 186 mm x 140 mm at x = 1.567 m. The measured velocity vector fields have spatial resolutions between 2.4 mm and 1.9 mm, with random errors between 15 mm/s and 12 mm/s. The LIF-measured flow depth has a random error less than 0.3mm. For the GV beach, the simultaneous velocity and depth measurements were repeated 15 times for each of the three measurement positions.

The ensemble-averaged depth at location x and time t was obtained from the LIF depth measurements via

$$\bar{h}(x,t) = \frac{1}{N}\sum_{i=1}^{N} h_i(x,t) \qquad (1)$$

where h_i is the LIF-measured depth for run i and N is the number of repeats of the experiment (N = 10 for CS and N = 15 for GV). Note that depth here refers to the distance from the instantaneous water surface to the top face of the PIV/LIF tower. The ensemble-averaged, depth-averaged velocity at location x and time t was obtained via

$$\overline{\langle u \rangle}(x,t) = \frac{1}{N}\sum_{i=1}^{N}\left\{\frac{1}{h_i}\int_0^{h_i} u_i(x,z,t)\,dz\right\} \qquad (2)$$

where angle brackets indicate depth averaging. For the remainder of the paper we use simply $u(t)$ and $h(t)$ to denote the ensemble-averaged, depth-averaged velocity and ensemble-averaged depth respectively. Figure 3 presents example depth and velocity measurements from individual runs and the corresponding ensemble-averaged results.

In addition to measuring depth at selected x locations, measurements were also made of the swash lens (swash lens being the term used for the instantaneous cross-shore profile of flow depth). This was achieved by mounting the laser above the flume in order to illuminate approximately 0.3 m of the water surface from above and using LIF to obtain the time-varying flow depth over the 0.3 m extent of the measurement with frequency 13.5 Hz (Kikkert et al., 2012). By moving the laser and LIF camera between repeats of the swash event, we obtain depth measurements for multiple 0.3 m-long cross-shore portions of the lens. Combining these measuremenst with each other, and with the depth measurements from the PIV-LIF locations, yields the swash lens measurement.

2.3 Sediment flux measurements

Intra-swash sediment flux was measured using sediment traps. Different traps were used for the uprush flux and the backwash flux. The uprush trap (Figure 2) comprises a net and timing mechanism that allows the net to be raised at a predetermined time. The net material was chosen to ensure sediment is trapped while keeping net porosity as high as possible: muslin and 2 mm nylon netting was used for CS and GV respectively. To minimise interference with the uprush flow, the net extended beyond the point of maximum run-up. The net was held in place by frames made from 1 mm-thick, 25 mm-wide aluminium bar; the frames were 204 mm high and 451 mm wide. Being slightly wider than the inside width of the flume, the good fit meant that no separate clamps were required, the trap was secure in the flow but sufficiently free to be rapidly lifted. The trap was placed with the bottom edge of its opening at a depth of 4-5 mm below the bed surface (corresponding to approximately $3.5d_{50}$ for the sand beach and $0.5d_{50}$ for the gravel beach). In the case of the gravel beach, individual particles are entrained by the flow and are bounced higher into the flow by collisions with neighbouring stationary particles; the result is that the gravel transport takes place above the initial mean bed level, not below. The trap was raised vertically using an electromagnet-controlled falling-weight mechanism connected to the front frame of the trap by steel wire and pulleys. The time of the trap lift was controlled by a pulse generator triggered by the lifting of the reservoir gate. The delay programmed into the pulse generator takes into account the time delay between the release of the trap weight and the lifting of the net. The delay was measured at each trap position using a reed switch at the trap linked to the gate reed switch and the pulse generator: the average of 10 measurements of the delay was taken. The uncertainty in the time between the release of the trap weight and the net being raised is the largest source of timing error; the standard deviation of the 10 measurements was taken as a measure of the uncertainty and was found to range between 0.002 and 0.010 s across the five trapping locations.

The intra-swash uprush sediment flux at a given x was measured by lifting the trap at different times for repeats of the swash event and measuring the (oven-dried) mass of sediment collected over the time interval. The uprush sediment flux for the i^{th} trapping period is then

$$q_s(i) = \frac{1}{w}\frac{1}{\rho_s}\left\{\frac{m(i)-m(i-1)}{t_L(i)-t_L(i-1)}\right\} \qquad (3)$$

where $t_L(i)$ and $t_L(i-1)$ are the trap lift times (s) for the i^{th} and previous time interval respectively; $q_s(i)$ is the mean sediment flux per metre flume width (m^3/s/m) over the time interval $t_L(i)-t_L(i-1)$; ρ_s = 2650 kg/m^3 is the sediment density; w = 0.45 m is the width of the flume; $m(i)$ and $m(i-1)$ are the masses (kg) of sediment collected during the i^{th} and previous time interval respectively; $t_L(i=0)=t_{ba}$ = the time of bore arrival and $m(i=0)$ = 0. The shortest time interval, corresponding to the time of bore arrival when flux is highest, was set at 0.2 s in order to ensure the interval time error does not exceed 5% (given a maximum uncertainty of 0.01 s in the timing).

The backwash trap (Figure 2) is box-shaped, open at the front and faces up the beach. It comprises an aluminium frame, steel wire mesh on the bottom and at the back, and muslin on the sides. The trap is 0.31 m high, 0.447 m wide (slightly narrower than the flume width) and 0.773 m long (sufficient to trap sediment entering at the front end). The trap is initially suspended above and parallel to the 1:10 beach face using a support structure attached to the top rails of the flume. Operation of the trap involved lowering to the bed at a prescribed time during the backrush, holding on the bed, and raising at a prescribed time. Trap lowering to the bed is achieved via a compressed air-driven actuator (SMC CD85N25-300-B, 1.0 MPa max pressure). The actuator has a solenoid-controlled valve to control the direction of compressed air, and a 5-port air control, including 2 exhaust ports, which controls the input pressure and hence the acceleration and deceleration of the trap. The actuator enables the trap to be lowered very quickly; four springs provide cushioning as the trap comes in contact with the beach surface. The extent to which the bottom edge of the trap goes below the bed surface level is not known for the backwash. In the case of the gravel the backwash flux was negligibly low. For the sand, the lower backwash velocities (compared to uprush) mean that only the surface layer of sand is mobilised in the backwash. The thickness of the edging on the trap is less than one sand grain size, so even if the trap sits on the beach surface with no penetration the sand flux enters the trap. Like the uprush trap, the backwash trap timing is controlled by a pulse generator, triggered by the lifting of the reservoir gate. At the moment of gate lifting, the reed switch triggers the pulse generator, which sends

two delayed pulses to the actuator, the first to lower the trap and the second to lift it. The delay programmed into the pulse generator for lowering the trap takes into account the time required for the trap to travel from its suspended position above the beach to the beach surface. The uncertainty in the time that the trap is on the beach surface is the largest source of error in the backwash timing. For this reason the trapping times are measured for each experiment individually via a micro-switch attached to one of the guiding rods. The switch is activated when the trap is within 3 mm of the beach surface; it therefore sends two pulses to the data acquisition system, one corresponding to the trap reaching the bed and the second corresponding to the lifting from the bed. Estimates for the error due to the variability in the down-time, as a percentage of the time the trap is on the beach surface, varied between 0.7 and 10.6%.

The intra-swash backwash sediment flux is calculated from

$$q_s(i) = \frac{1}{w}\frac{1}{\rho_s}\left\{\frac{m(i)}{t_{up}(i) - t_{dn}(i)}\right\} \qquad (4)$$

where $t_{dn}(i)$ and $t_{up}(i)$ are the times (s) of trap lowering and raising respectively; $q_s(i)$ is the mean sediment flux per unit flume width ($m^3/s/m$) over the time interval $t_{up}(i) - t_{dn}(i)$ and $m(i)$ is the mass (kg) of sediment collected during the time interval.

For the CS beach, uprush and backwash sediment flux measurements were made at four cross-shore locations, at x = 0.602, 1.447, 2.286 and 3.117 m (the locations of the sediment flux measurements were slighty seaward of the PIV-LIF measurements in order to avoid the perspex towers). At each location, uprush and backwash flux was measured for 5 time intervals (except at x = 3.117 m for which backwash flux was measured for 3 time intervals), and measurements were repeated 3 to 6 times.

For the GV beach, uprush sediment flux measurements were made at x = 0.602, 1.447 and 2.286 m; the lower maximum run-up on the gravel beach precluded measurements at higher x. At x = 0.602 and 1.447 m, the uprush flux was measured for 5 time intervals, with 3 to 4 repeats of each measurement; for x = 2.286 m, the uprush flux was measured over one time interval only because of the short duration of the swash at this position. No backwash flux measurements were made for GV because backwash flux was negligible at all measurement locations in this case.

Table 1 presents the details of the sediment flux measurements: 176 measurements were made in total, covering four x-locations for CS and three x-locations for GV, with typically five intra-swash times at each location and typically four repeats of each measurement. Note that the beach was fully drained to the initial 62 mm groundwater level and restored to its 1:10 uniform slope between each run.

3.0 EXPERIMENTAL RESULTS: HYDRODYNAMICS

3.1 Shoreline motion and maximum runup

The swash lens measurements have been analysed to determine shoreline motion through the swash cycle, with instantaneous shoreline position defined as the cross-shore location where the instantaneous lens depth is 5 mm (Kikkert et al., 2012). The ensemble-averaged shoreline trajectories for the mobile CS and GV beaches are presented in Figure 4, along with the shoreline trajectory results from the corresponding immobile, impermeable and immobile, permeable beach experiments reported by Kikkert et al. (2012, 2013).

Shoreline motion for the mobile CS beach (Figure 4a) is similar to that for the corresponding immobile beaches during the first 1 s following bore arrival. Within this time the shoreline advances approximately 2.3 m. Thereafter shoreline deceleration increases as the shoreline approaches maximum run-up. The deceleration is higher and the maximum run-up correspondingly lower for the mobile CS beach compared to the immobile beaches: maximum run-up is 3.95 m, reached at 5.33 s, compared with a maximum run-up of 4.33 m and 4.53 m for the immobile permeable and immobile impermeable beaches respectively. There is therefore a 13% reduction in maximum run-up between the immobile, impermeable beach and the mobile beach, with two thirds of this reduction arising from bed mobility and one third from bed permeability. For the relatively low-permeability CS beach therefore, the effect of bed mobility is more significant than the effect of bed permeability in terms of maximum run-up. Backwash shoreline motion is similar for the three beaches, although the speed of shoreline retreat is a little higher for the mobile and permeable beaches compared to that of the impermeable beach: an average speed of approximately 1.5 m/s for $t \geq 7$ s on the mobile and permeable beaches compared with an average speed of 1.3 m/s for the impermeable beach. The slightly higher retreat speed is likely due to infiltration into the mobile and permeable beaches during backwash (as discussed by Steenhauer et al. (2011) and Kikkert et al. (2013), 33% of the water volume crossing x = 0.072 m infiltrates the CS permeable beach, with 13% of this infiltration occurring during the backwash).

Figure 4(b) shows the measured shoreline trajectory for the mobile GV beach. The trajectory is similar to that of the corresponding immobile, permeable beach (except close to maximum run-up, between 3.5 and 4.5 s), but it is very different to that of the corresponding immobile impermeable beach. Infiltration is much greater for the GV beach compared with the CS beach, with 45% of the water volume that crosses x = 0.072 m infiltrating the GV beach during uprush (Steenhauer et al., 2011). Maximum run-up on the mobile beach is 2.7 m, occurring at 4.5 s, compared with a maximum run-up of 2.93 m and 3.95 m on the immobile permeable and impermeable beaches respectively. For GV therefore, the effects of permeability on shoreline motion are much more significant than the effects of bed mobility: maximum run-up on the mobile beach is 32% lower than maximum run-up on the corresponding immobile, impermeable beach, with 26% of this being due to the permeability.

3.2 Swash depths

Figure 5 presents swash lenses for twelve intra-swash times on the CS beach and Figure 6 presents the ensemble-averaged depth time-series for the five (u,h) measurement locations. The lenses and depth time-series for the GV beach are presented in Figures 7 and 8.

In the case of CS, the lenses and depth time-series for the mobile beach are similar to those of the immobile permeable and impermeable beaches. Significant differences in the lenses are seen only at times close to maximum uprush (i.e. between 4.52 and 6 s), when the mobile bed lenses tend to be lower than the immobile bed lenses; significant differences in the depth time-series are seen only at locations far up the beach slope (x = 3.177 m in Figure 6), where mobile bed depths are lower than the immobile bed depths. These results are consistent with the results for shoreline trajectory seen in Figure 4, and are also consistent with the hypothesis that bed mobility serves as an added momentum sink through an increase in the effective bed roughness and through fluid-particle interactions.

In the case of GV (Figures 7 and 8), the high permeability of the mobile and immobile permeable beaches results in the swash lenses for these beaches being very different to those of the immobile impermeable beach: the lenses for the mobile and permeable beaches are lower than those of the impermeable beach and extend much less far up the beach (lower maximum run-up). At the same time, the mobile bed and permeable bed lenses are rather similar (but not the same), underlining the earlier result that the effects of bed permeability are more significant than the effects of bed mobility in the case of GV. Differences in swash depth between the mobile and the immobile, permeable beaches are seen in the region x > 1 m, where depths on the mobile beach are up to 20 mm higher

than on the the immobile, permeable beach during the later uprush. The reason for the difference is likely related to the fact that gravel entrained lower down the slope tends to deposit in this region during uprush, thereby increasing the bed level and forcing the free surface upwards by an amount equivalent to 1 – 2 sediment grain diameters.

3.3 Swash velocities

The depth-averaged velocity measurements are presented in Figures 9 and 10. For the CS beach (Figure 9), except far up the beach, uprush velocities for the mobile beach are similar to those of the immobile beaches in terms of the timing and magnitude of the maximum velocity, the flow deceleration and the timing of flow reversal. Noticeable differences occur in the backwash, with backwash velocities for the mobile beach and the immobile permeable beach being lower than backwash velocities on the impermeable beach. Also, the mobile beach backwash velocities are lower than the permeable beach backwash velocities for three of the five measurement locations. The difference at x = 3.177 m reflects the lower maximum runup on the mobile beach, while the lower backwash velocities at x = 0.072 and 1.567 m may be an effect of an increase in the effective bed roughness and momentum loss to fluid-sediment interactions, as more sand becomes mobile during the later stages of the backwash.

Figure 10 presents the depth-averaged velocity time-series for the three measurement locations on the GV mobile beach. As for the GV shoreline trajectories, the results are dominated by the effects of permeability, with backwash velocities on the mobile and immobile permeable beaches being much lower than those on the impermeable beach. Backwash velocities are low in the case of the GV mobile beach - up to a factor of 2 lower compared with the CS mobile beach – which means there is limited capacity for backwash sediment mobility in the case of the GV beach.

4.0 EXPERIMENTAL RESULTS: SEDIMENT FLUX

Figure 11 presents the processed flux results. The figure shows the intra-swash sediment flux for the four flux measurement locations on the CS beach and the three flux measurement positions on the GV beach. All 176 individual flux measurements are shown (although not all are visible because of overlapping results); the average flux at each x and t is indicated by the horizontal line, the length of which indicates the sediment trapping time interval for the measurement. The transported masses of sediment are substantial: the highest uprush mass recorded was approximately 3.5 kg, occurring at x = 1.447 m on the GV beach; this equates to a 7.8 kg/m uprush mass, which is comparable to uprush masses measured in the field (Blenkinsopp et al., 2011). (Note that a subset of the CS data was reported by Briganti et al. (2012) and used thereafter by Hu et al. (2015); the results presented here

constitute the entire experimental dataset for the two beaches and contain corrections to the bore arrival times and, consequently, to the sediment flux at bore arrival reported in Briganti et al. (2012)).

There is generally good agreement between individual flux measurements for given x and t and the results are consistent in terms of their variation with x and t, and consistent with visual observations made during the experiments. For each x the sediment flux is highest at the time of bore arrival, decays rapidly with time thereafter and reaches zero at some time before flow reversal. Peak uprush flux is much higher for GV than for CS – a factor 2 higher approximately - consistent with a higher bed shear stress arising from the rougher bed. In the backwash, the flux is slow to build up as the flow accelerates down the beach. For the GV beach, the backwash sediment flux is negligibly small. For the CS beach the backwash flux peaks at about the time of maximum backwash velocity; peak backwash flux is higher and occurs later in time for lower locations on the beach, consistent with the backwash velocities. No sediment was transported off the beach onto the horizontal bed between the gate and the beach. This is because the supercritical backwash flow jumps to subcritical below the initial shoreline location (but still on the slope) at the end of the backwash, with the result that particles in suspension settle to the bed, raising the bed elevation in this region by a few millimetres in the case of the CS beach and by order of a grain size in the case of the GV beach (note that bed elevation was not measured). This is consistent with the creation of a bed-step at a backwash bore as described by Zhu and Dodd (2015). In addition to the accretion observed below the initial shoreline, accretion also occurred in the mid-to-upper swash, reaching an estimated (not measured) maximum of order of a few millimeters in the case of CS and of one grain size in the case of GV. After each swash run the sediment was re-distributed to restore the 1:10 beach slope by matching the beach surface to the lines marked on the glass sides of the flume.

5.0 SEDIMENT TRANSPORT CALCULATION

In Section 5.2 we apply a sediment transport formula to the experimental conditions: we take the measured hydrodynamics as input to the transport formula and compare the formula-calculated intra-swash sediment flux with the measured flux. Because the sediment transport formula is bed shear stress-based, we first give some consideration to estimating bed shear stress for swash flow.

5.1 Swash bed shear stress

We assume the instantaneous bed shear stress, τ_b, relates to the instantanteous flow through

$$\tau_b = \frac{1}{2}\rho f_b u|u| \qquad (5)$$

where ρ is the water density (1000 kg/m^3) and f_b is the bed friction factor. For steady flows and oscillatory flows, f_b depends on Reynolds number and relative roughness, and there are well-established methods for estimating f_b for such flows. Swash bed shear stress is complicated by the flow's high unsteadiness and non-uniformity. Measurements of intra-swash bed shear stress have been obtained by Conley and Griffin (2004) using a hot-fim sensor at a field site, by Barnes et al. (2009), Pujara et al. (2015) and Jiang and Baldock (2015) using a shear plate on laboratory impermeable and mobile slopes, and by Kikkert et al. (2012, 2013) using log-law fitting to PIV-measured velocity profiles over laboratory impermeable and permeable beaches. Such measurements have yet to result in a predictive formula for intra-swash bed shear stress.

In the absence of an established predictor, here we estimate f_b using two methods. The first is based on the Swart formula (1974) commonly used to calculate friction factor for wave-driven oscillatory flow conditions. The approach was previously used by Othman et al. (2014) to estimate friction factor for their laboratory overwash experiments and by Masselink and Turner (2012) for swash flows in field conditions. The Swart formula is

$$f_b = 0.0025\exp\left[5.213\left(\frac{a}{k_s}\right)^{-0.194}\right] \qquad (6)$$

where a is the amplitude of the oscillatory flow water particle displacement and $k_s = 2.5d_{50}$ is the bed roughness, with d_{50} the sediment size. Applied to swash, we estimate a from

$$a = \frac{T_s}{\sqrt{2}\pi}u_{sd} \qquad (7)$$

where u_{sd} is the standard deviation of $u(t)$ at a given x location in the swash zone and $T_s = t_{end} - t_{ba}$ is the swash "period", with t_{ba} being the time of bore arrival at x and t_{end} the time corresponding to the end of the swash at x (when the backwash velocity is zero). Substitution for a in equation (6) yields a time-invariant f_b for the given x location. Of course, the applicability of Swart to swash flow is questionable: for Swart the near-bed hydrodynamics are established over multiple flow cycles and the flow depth is much greater than the oscillatory boundary layer thickness. In contrast, here we

have a single flow "cycle" with peak velocity occurring at the start of the cycle and flow depth varying and becoming very shallow in the late backwash.

A disadvantage of Swart in the context of predictive modelling is the need to know the swash period T_s and the velocity standard deviation u_{sd} *a priori*. The second method used to estimate f_b is the Colebrook formula which calculates instantaneous f_b based on the instantaneous flow depth and velocity:

$$\frac{1}{\sqrt{\lambda}} = -2\log_{10}\left(\frac{k_s}{3.7D_h} + \frac{2.51}{\mathrm{Re}\sqrt{\lambda}}\right) \qquad (8)$$

where $\lambda = 4f_b$, $D_h = 4h$ and $\mathrm{Re} = \frac{uh}{\nu}$ is Reynolds number, with ν being the water kinematic viscosity. Again, the applicability of Colebrook for estimating swash flow f_b is questionable for a number of reasons. First, the Colebrook formula is applicable to conditions in which the boundary layer is fully developed, a condition that is unlikely to be met at, and soon after, the time of bore arrival at a location on the beach. Second, the Colebrook formula applies to turbulent flow, a condition that is not met close to the time of flow reversal (in addition, Re = 0 at flow reversal, giving a singularity for f_b at this time) and towards the very end of the backwash (when both flow depth and flow velocity are low); this is a minor concern however in the context of estimating intra-swash sediment flux because the percentage of the swash duration for which the flow is not turbulent is small (less than 5% in the mid-swash) and velocities are very low at these times. Third, in the late backwash a fully-developed boundary layer cannot occur because of the limited water depth as the flow becomes increasingly shallow; a Lagrangian-type model as suggested by Barnes and Baldock (2010) may be more appropriate at this stage of he swash. Moreover, in the extreme late backwash, when the flow depth is extremely shallow, the flow regime becomes akin to flow over obstacles rather than a boundary layer flow condition.

To compare the two methods with each other, and to evaluate them against experimental data, we apply the methods to the experimental data of Kikkert et al. (2013), who measured swash depths and velocities at four cross-shore locations on immobile, permeable coarse sand and gravel beaches and obtained estimates of the intra-swash bed shear stress at each location based on log-law fitting to the measured velocity profiles. Here we take the measured depth and velocity time-series as input to the Swart and Colebrook calculations. At each cross-shore measurement location the measurements give t_{ba} and $u(t)$, $h(t)$ for $t_{ba} < t < t_{end}$ (u and h cannot be

accurately measured at, and immediately following, the moment of bore arrival because of air bubbles in the arriving bore front). The measured data are processed as follows to give $u(t)$ and $h(t)$ spanning the full swash period from $t = t_{ba}$ to $t = t_{end}$: (i) set t_{end} equal to the time of the last (u,h) measurement plus one measurement timestep; (ii) extrapolate the measured $u(t)$ to find $u(t = t_{ba})$ and set $u(t = t_{end}) = 0$; (iii) extrapolate the measured $h(t)$ to find $h(t = t_{ba})$ and set $h(t = t_{end})$ equal to the last measured depth; (iv) interpolate to get $u(t)$ and $h(t)$ at 200 evenly-spaced times between t_{ba} and t_{end} . An example calculation is shown in Figure 12: it takes Kikkert et al.'s (2013) measured $u(t)$ and $h(t)$ at x = 0.772 m on their coarse sand beach as input and calculates f_b and τ_b using Swart and Colebrook. The Swart f_b is time-invariant with, for this example, a value of 0.0125. The Colebrook f_b is time-varying and lower than Swart f_b for most of the swash; the lowest Colebrook f_b for this example is 0.0085, approximately 0.7 times the Swart f_b , and occurs around midway during the uprush when the flow depth is a maximum and the Colebrook relative roughness $\frac{k_s}{D_h}$ is a minimum. In the late backwash the flow depth becomes shallow, leading to a rapid increase in the relative roughness and to Colebrook f_b reaching twice the value of Swart f_b . The differences between Swart and Colebrook f_b are reflected in the calculated bed shear stresses, $\tau_b(t)$, shown in the bottom panel of Figure 12. Note that the large difference in f_b in the late backwash translates to a relatively small absolute difference in τ_b because of the low velocities at this time.

Figure 13 shows the Swart- and Colebrook-calculated $\tau_b(t)$ obtained using the measured depths and velocities for all four locations on Kikkert et al.'s (2013) coarse sand and gravel beaches; Kikkert et al.'s log-law-based estimates of $\tau_b(t)$ are also shown. A comparison between the Swart and Colebrook bed shear stresses (τ_{bS} and τ_{bC} respectively) is presented differently in Figure 14 by plotting τ_{bS} versus τ_{bC} . The results show that τ_{bS} is generally greater than τ_{bC} during uprush; the ratio of τ_{bS} to τ_{bC} in the uprush lies in the range $0.9 < \left.\frac{\tau_{bS}}{\tau_{bC}}\right|_{up} < 1.7$ across all locations on the two beach types, with the value of the ratio mainly dependent on cross-shore position. In the early backwash τ_{bS} and τ_{bC} are in close agreement, while in the late backwash τ_{bC} becomes increasingly greater than τ_{bS} ; the ratio of τ_{bS} to τ_{bC} in the backwash lies in the range $0.5 < \left.\frac{\tau_{bS}}{\tau_{bC}}\right|_{back} < 1.1$ for CS and in the range $0.25 < \left.\frac{\tau_{bS}}{\tau_{bC}}\right|_{back} < 1.1$ for GV, with the value of the ratio mainly dependent on time in the backwash.

In Figure 13, Kikkert et al.'s (2013) experimental results for $\tau_b(t)$, based on log-law fitting to the measured velocity profiles, show the same general behaviour as Colebrook and Swart – decreasing τ_b during uprush, increasing in the early backwash and decreasing again in the late backwash – but the results show significant scatter and varying level of agreement with Swart- and Colebrook-calculated τ_b , depending on position on the beach and depending on uprush or backwash. Figure 15 shows the comparison by plotting calculated τ_b (taken as the mean of τ_{bS} and τ_{bC}) against experimental τ_b . The calculated τ_b lies mostly within a factor 2 of the experimental values for both beaches, but tends to be higher than the experimental τ_b during uprush and much lower in the late backwash. Note that the experimental results cannot be taken as ground truth in this comparison because the unsteady and non-uniform nature of the flow means that the validity of the log law is questionable and its practical application difficult, which may explain some of the scatter in the experimental results. We note that a previous comparison of log-law-based measurements of swash bed shear stress over impermeable beds showed reasonable agreement with corresponding shear plate measurements for uprush, but very poor agreement in the backwash, with the log-law backwash estimates being much higher than the shear plate backwash estimates (O'Donoghue et al., 2010).

5.2 Intra-swash sediment flux

Given the relatively large sediment size, the sediment flux is treated as bedload with the Meyer-Peter and Müller formula used to estimate the instantaneous flux, i.e.

$$q_s = C\sqrt{\left(s_g - 1\right) g d_{50}^3}\left(\left|\theta\right| - \theta_{cr}\right)^{1.5}\frac{\left|\theta\right|}{\theta} \qquad (9)$$

where C is a constant, s_g = 2.65 is sediment specific weight, g is acceleration due to gravity and $\theta = \dfrac{\tau_b}{\rho\left(s_g - 1\right) g d_{50}}$ is instantaneous non-dimensional bed shear stress, with water density ρ = 1000 kg/m^3; θ_c is the non-dimensional bed shear stress corresponding to the threshold of sediment motion and is here calculated in the same way as in Othman et al. (2014), including an adjustment for the bed slope. We process the measured $u(t)$ and $h(t)$ from the present mobile bed experiments in the same way as previously described, calculate $\tau_b(t)$ via the Swart and Colebrook formulae and use equation (9) to obtain two estimates of the intra-swash sediment flux, $q_s(t)$, one based on the Swart-

calculated $\tau_b(t)$ and the other based on the Colebrook-calculated $\tau_b(t)$. In applying Swart and Colebrook we make no allowance for the fact that the bed is now mobile, even though the presence of a moving sediment layer may increase the bed shear stress somewhat (Jiang and Baldock, 2015). For steady flows, a value of 8 is normally used for the constant C in the Meyer-Peter and Müller formula; here we adopt C = 12, as is often used in the case of unsteady and oscillatory flows (e.g. Nielsen, 2006). Note that the choice of value for C (12 or 8) generally has a similar level of impact on the calculated instantaneous flux as the choice of Swart or Colebrook for the friction factor.

Figure 16 presents the calculated and measured intra-swash flux for four locations on the CS beach and two locations on the GV beach (flux measurements at the third flux-measurement location on the GV beach give only one point for the time-series). The experimental results shown are the averaged results from Figure 11 and include a horizontal line to indicate the trapping time interval for the measurement. For the purpose of comparing the measured and calculated flux, we ignore the difference (approximately 0.1 m) in the position of the sediment flux and the position of the hydrodynamic measurements: i.e. we assume the flux measured at the location adjacent to the (u,h) measurement location can be attributed to the (u,h) measurement location.

In Figure 16, uprush sediment flux based on Colebrook is always lower than that based on Swart, reflecting the differences already seen between Swart- and Colebrook-calculated f_b for uprush; the differences are more apparent for q_s than for τ_b because of the higher power dependence of q_s on f_b ($\tau_b \propto f_b, q_s \propto f_b^{1.5}$) . With the exception of x = 1.567 m for the GV beach, there is good agreement between the Colebrook- and Swart-based estimates of the peak uprush flux at the time of bore arrival; the large difference at x = 1.567 m on the gravel beach is due to the relatively low value of a at this location, which increase τ_{bS} relative to τ_{bC} . In the backwash, the Colebrook and Swart estimates are in good agreement in the early backwash; differences become apparent in the late backwash when high Colebrook friction factors result in higher q_s compared to the Swart q_s.

As shown in Figure 17, uprush flux calculated using Swart and Colebrook generally lies within a factor 2 of the measured uprush flux. In some cases (e.g. CS, x = 2.377 m) the level of agreement between the measured and calculated uprush flux is remarkably good. Agreement is generally poor in the backwash. For the CS beach, there is reasonable agreement in terms of the magnitude of the peak backwash flux (at least compared to Swart), but there is discrepancy in the timing of the peak and of the backwash flux generally: the calculated backwash flux is generally higher than the measured flux

early in the backwash, it peaks sooner and is lower than the measured flux late in the backwash. In the case of GV, the measured backwash flux is negligibly small but the calculated q_s show a small backwash flux at x = 1.567 m and significant backwash flux at x = 0.772 m. This difference between calculated and measured backwash q_s for GV is at odds with the backwash bed shear stress results for GV seen in Figure 13, in which the measured backwash bed shear stresses at these x are similar to or higher than the calculated bed shear stress. A possible explanation is that both the calculated and log-law-based measures over-estimate the actual bed shear stress in the backwash. Another possibility is that the flux is limited by flow depth. In the late backwash when velocity is high, the flow depth is shallow and rapidly decreasing. For example, in the case of GV, x = 0.772 m, the bulk of the calculated backwash flux occurs in the time period 6 < t < 8 s, during which time the flow depth decreases from 75 mm to 10 mm, i.e. from about 9 grain diameters depth to about 1 grain diameter depth. It is unlikely that such shallow flows have the capacity to convey the bedload normally associated with bed shear stress levels indicated by the calculated and measured backwash bed shear stresses.

While C = 12 in the Meyer-Peter and Müller formula gives good estimates of the uprush flux for the present experiments, we note that Othman et al. (2014) report C in the range 22 – 42 (Table 7 in Othman et al., 2014) when they apply Meyer-Peter and Müller to their measurements of sediment load overwashing a truncated slope, with bed shear stress estimated using various methods, including Swart and Colebrook. The difference in C between the present study and Othman et al. (2014) may be due to error in estimating the uprush bed shear stress, in the present study and/or in Othman et al. (2014): the difference in C between the two studies is of order factor 3, which would correspond to a factor 2 difference in the bed shear stress. The difference in C may also be due (wholly or partly) to the difference in the experimental set-up: while the present experiments involve sediment flux measurements over a continuous and deep sediment beach, Othman et al. (2014) measured the sediment volume overwashing a truncated slope comprising a shallow (20 mm) sediment bed on a hard surface.

5.3 Net volume transport

Figure 18 presents the measured and calculated total sediment volume transported during uprush and backwash at each location on the two beaches. The measured volumes in Figure 18 are simply the volumes of sediment collected when the trap was in position for the whole of the uprush or backwash duration; the calculated volumes are obtained from the integral of the uprush and backwash flux time-

series for all five (u,h) measurement locations on the CS beach and all three (u,h) measurement locations on the GV beach.

For the CS beach, the measured uprush and backwash volumes decay monotonically with distance up the beach for x > 0.6 m, which means this stretch of beach is accreting during uprush and eroding during backwash. Uprush accretion is lower in the lower swash compared to the mid and upper swash, while backwash erosion is highest in the mid-swash and low in both the lower and upper swash. The net result over the full swash event is accretion in the lower swash, no change in the mid-swash and net accretion in the upper swash. Note that the net volume changes are small: if converted to a mean bed level change over the region, the result is approximately 0.25 mm accretion in the lower swash and approximately 1 mm accretion in the upper swash. For the CS beach, the calculated volumes agree reasonably well with each other and with the measured volumes, echoing the level of agreement seen in the uprush flux time-series in Figure 16. A difference between the measured and calculated volumes is the higher calculated uprush volume at x = 1.567 m, implying erosion between x = 0.772 m and x = 1.567 m, as opposed to the accretion implied by the measured volumes. At x = 0.072 m the calculated uprush volumes are low compared to the volumes at x = 0.772 m because at this x the bore has relatively large depth (Figure 6) and low velocity (Figure 9), being so close to the initial shoreline position where the bore has not yet fully collapsed onto the beach. The calculated volumes imply uprush erosion, backwash accretion and net erosion in this very low region of the swash (consistent with observations made during the experiment). Note that the difference in the Swart-based and Colebrook-based estimates of uprush volume is larger at x = 0.072 m compared to elsewhere on the beach because the large depth at this location increases the Colebrook relative roughness, thereby decreasing the Colebrook friction factor, as previously discussed.

The measured volumes for the GV beach indicate uprush erosion in the lower swash region, uprush accretion in the upper swash region and no change in the backwash, although with only three measurement positions the trends are not well resolved. The net volume changes are again small: converted to a mean bed level change, the result is approximatley 1.5 mm erosion in the lower swash and approximately 4 mm in the upper swash. The calculated uprush volumes show a similar trend to the measured uprush volumes – erosion in the lower swash followed by accretion in the upper swash – but there is greater discrepancy between the measured and calculated volumes compared to CS, and greater discrepancy between Swart and Colebrook compared to CS; the discrepancy between Swart and Colebrook is largest at x = 0.072 m where, again, the large depth results in lower Colebrook friction factor compared with Swart. In the backwash the measured volumes were negligibly small

(indicated as zero in Figure 18) while the calculated volumes imply increasing backwash erosion over the full swash region.

6.0 CONCLUSION

Dambreak-type swash experiments have been conducted in which intra-swash hydrodynamics and sediment flux have been measured for swash on mobile coarse sand and gravel beaches. The following are the main conclusions:

(i) Apart from the bed mobility, the experimental set-up is the same as for the immobile, permeable beach experiments of Kikkert et al. (2013), which enables the effects of sediment mobility on the swash hydrodynamics to be quantified. The results indicate that bed mobility impacts on the hydrodynamics, reducing the maximum run-up by approximately 8% for both beaches compared to maximum run-up on the corresponding immobile beach. For the sand beach, the effect of bed mobility on the uprush hydrodynamics seems to be more significant than the effect of bed permeability, while for the gravel beach the effects of permeability are dominant.

(ii) The measured intra swash sediment flux at a given location in the swash zone is characterised by high flux at the moment of bore arrival, followed by rapid decay during uprush, becoming zero at some time before flow reversal. The highest uprush flux on the gravel beach is approximately a factor 2 higher than the highest uprush flux on the sand beach. For the gravel beach, the backwash sediment flux is negligibly small, while for the sand beach the backwash flux increases slowly as the flow accelerates down the beach, and peaks at about the time of maximum backwash velocity.

(iii) Uprush bed shear stress estimated using Swart is generally higher than that estimated using Colebrook; for the swash conditions considered in this study, the ratio $\left.\frac{\tau_{bS}}{\tau_{bC}}\right|_{up}$ reached a maximum value of 1.7, occurring in the lower swash where uprush flow depth is largest. In the backwash, Colebrook-estimated bed shear stress becomes increasingly greater than Swart-estimated bed shear stress; for the swash conditions considered in the present study, the maximum value of $\left.\frac{\tau_{bS}}{\tau_{bC}}\right|_{back}$ was approximately 2 for the CS beach and 4 for the GV beach.

(iv) Bed shear stresses calculated using Swart and Colebrook lie mostly within a factor 2 of the swash bed shear stress estimates obtained by Kikkert et al. (2013) using log-law fitting to velocity profiles measured over immobile permeable beaches. For uprush, the calculated bed

shear stresses tend to be higher than the experimental values; in the backwash, the experimental peak bed shear stresses are a factor 2 higher than the calculated values (but we note that a previous comparison of log-law-based estimates of bed shear stress with shear plate measurements also showed poor agreement in the backwash, with the log-law backwash estimates being much higher than the shear plate backwash estimates).

(v) Intra-swash sediment flux calculated using the Meyer-Peter and Müller bed load transport formula, with bed shear stress estimated using Swart or Colebrook, are generally within a factor 2 of the measured intra-swash flux. The agreement between the calculated and measured flux is better for the sand beach than for the gravel beach, and better for uprush than for backwash. For the sand beach there is good agreement between the calculated and measured total uprush and total backwash sediment volumes. The agreement is less good for the gravel beach, for which the calculated and measured uprush volumes show a similar trend but the calculated backwash volumes over-estimate the (negligible) volumes observed in the experiments.

The measurements from the present study constitute a unique but limited dataset on intra-swash sediment flux: more experiments are needed to cover a greater range of swash and sediment conditions, including finer sediments for which the effects of flow unsteadiness and non-uniformity are likely to be substantial. More work is also needed to formulate a robust bed shear stress model that is able to cover the wide range of hydrodynamic conditions occurring across the full swash zone and through the full swash cycle. Finally, the experimental data are available on request to the first author.

ACKNOWLEDGEMENTS

The research reported in this paper was conducted as part of a collaborative research project involving the Universities of Aberdeen and Nottingham in the UK, funded by the UK's Engineering and Physical Sciences Research Council (EPSRC grants EP/E011330/1 and EP/E010407/1). Riccardo Briganti acknowledges support through an EPSRC Career Acceleration Fellowship (EP/I004505/1). The paper has benefitted from the helpful comments provided by Professor Tom Baldock and an anonymous reviewer.

REFERENCES

Alsina, J.M. and I. Caceres, 2011. Sediment suspension events in the inner surf and swash zone. Measurements in large-scale and high-energy wave conditions. Coastal Engineering, 58, 657-670.

Alsina, J.M., Caceres, I., Brocchini, M. and T. E. Baldock, 2012. An experimental study on sediment transport and bed evolution under different swash zone morphological conditions. Coastal Engineering, 68, 31-43.

Austin, M.J., and G. Masselink, 2006. Observations of morphological change and sediment transport on a steep gravel beach. Marine Geology, 229 (1-2), 59-77.

Baldock, T. E., Alsina, J.M., Caceres, I., Vicinanze, D., Contestabile, P., Power, H. and A. Sanchez-Arcilla, 2011. Large-scale experiments on beach profile evolution and surf and swash zone sediment transport induced by long waves, wave groups and random waves. Coastal Engineering, 58, 214-227.

Barnes, M.P. and T.E. Baldock, 2010. A Lagrangian model for boundary layer growth and bed shear stress in the swash zone. Coastal Engineering, 57 (4), 385-396.

Barnes, M.P., O'Donoghue, T., Alsina, J.M. and T.E. Baldock, 2009. Direct bed shear stress measurements in bore-driven swash. Coastal Engineering, 56 (8), 853-867.

Blenkinsopp, C.E., Turner, I.L., Masselink, G. and P.E. Russell, 2011. Swash zone sediment fluxes: Field observations. Coastal Engineering, 58 (1), 28-44.

Briganti, R., Dodd, N., Pokrajac, D. and T. O'Donoghue, 2012. Numerical and experimental description of the flow, boundary layer and bed evolution in bore-driven swash on a coarse sediment beach. Coastal Engineering Proceedings, 1:33, doi: http://dx.doi.org/10.9753/icce.v33.currents.33 .

Caceres, I. and J. M. Alsina, 2012. A detailed, event-by-event analysis of suspended sediment concentration in the swash zone. Continental Shelf Research, 41, 61-76.

Conley, D. C. and J. G. Griffin Jr., 2004. Direct measurements of bed stress under swash in the field. J. Geophys. Res., 109, C03050, doi:10.1029/2003JC001899

Cowen, E.A., Sou, I.M., Liu, P.L.-F. and B. Raubenheimer, 2003. Particle image velocimetry measurements within a laboratory-generated swash zone. Journal of Engineering Mechanics, 129(10), 1119-1129.

Gedik, N., Irtem, E. and S. Kabdasli, 2005. Laboratory investigation on tsunami run-up. Ocean Engineering, 32(5-6), 513-528.

Hu, P., Li, W., He, Z., Phtz, T. and Z. Yue, 2015. Well-balanced and flexible morphological modeling of swash hydrodynamics and sediment transport. Coastal Engineering, 96 (0), 27–37.

Hughes, M.G., Masselink, G. and R.W. Brander, 1997. Flow velocity and sediment transport in the swash zone of a steep beach. Marine Geology, 138 (1-2), 91-103.

Jiang, Z and T. E. Baldock, 2015. Direct bed shear stress measurements under loose bed swash flows. Coastal Engineering, 100, 67-76.

Kikkert, G.A., O'Donoghue, T., Pokrajac, D. and N. Dodd, 2012. Experimental study of bore-driven swash hydrodynamics on impermeable rough slopes. Coastal Engineering, 60 (0), 149–166.

Kikkert, G.A., Pokrajac, D., O'Donoghue, T., and K. Steenhauer, 2013. Experimental study of bore-driven swash hydrodynamics on permeable rough slopes. Coastal Engineering, 79, 42-56.

Masselink, G. and M.G. Hughes, 1998. Field investigation of sediment transport in the swash zone. Continental Shelf Research, 18 (10), 1179-1199.

Masselink, G., Russell, P., Turner, I. and C. Blenkinsopp, 2009. Net sediment transport and morphological change in the swash zone of a high-energy sandy beach from swash event to tidal cycle time scales. Marine Geology, 267 (1-2), 18-35.

Masselink, G. and I. L. Turner, 2012. Large-scale laboratory investigation into the effect of varying back-barrier lagoon water levels on gravel beach morphology and swash zone sediment transport. Coastal Engineering, 63, 23-38.

Nielsen, P. and D. P. Callaghan, 2006. Shear stress and sediment transport calculations for sheet flow under waves. Coastal Engineering, 47 (3), 347-354.

O'Donoghue, T., Pokrajac, D. and L. Hondebrink, 2010. Laboratory and numerical study of dambreak-generated swash on impermeable slopes. Coastal Engineering, 57 (5), 513 – 530.

Othman, I.K., Baldock, T.E. and D.P. Callaghan, 2014. Measurement and modelling of the influence of grain size and pressure gradient on swash uprush sediment transport. Coastal Engineering, 83, 1-14.

Petti, M. and S. Longo, 2001. Turbulence experiments in the swash zone. Coastal Engineering, 43(1), 1-24.

Pujara, N., L.-F. Liu, P. and H. Yeh, 2015. The swash of solitary waves on a plane beach: flow evolution, bed shear stress and run-up. J. Fluid Mech., 779, 556-597.

Puleo, J. A., Lanckriet, T., Conley, D. and D. Foster, (in press). Sediment transport partitioning in the swash zone of a large-scale laboratory beach. Coastal Engineering.

Rivillas-Ospina, G., Pedrozo-Acuna, A., Silva, R., Torres-Freyermuth, A. and C. Gutierrez, 2012. Estimation of the velocity field induced by plunging breakers in the surf and swash zones. Experiments in Fluids, 52, 53-68.

Shin, S. and D. Cox, 2006. Laboratory observations of inner surf and swash-zone hydrodynamics on a steep slope. Continental Shelf Research, 26 (5), 561-573.

Sou, I.M., Cowen, E.A. and P.L.-F. Liu, 2010. Evolution of the turbulence structure in the surf and swash zones. Journal of Fluid Mechanics, 644, 193-216.

Steenhauer, K., Pokrajac, D., O'Donoghue, T. and G.A. Kikkert, 2011. Subsurface processes generated by bore-driven swash on coarse-grained beaches. Journal of Geophysical Research: Oceans, 116 (4), art. no. C04013.

Swart, D.H., 1974. Offshore sediment transport and equilibrium beach profiles. Delft Hydr. Lab. Publ., No.131, Delft Hydraulics, The Netherlands.

Van der Zanden, J., Alsina, J.M., Caceres, I., Buijsrogge, R. and J.S. Ribberink, 2015. Bed level motions and sheet flow processes in the swash zone: observations with a new conductivity-based concentration measuring technique (CCM^{+}). Coastal Engineering, 105, 47-65.

Zhu, F. and N. Dodd, 2015. The morphodynamics of a swash event on an erodible beach. Journal of Fluid Mechanics, 762, 110-140.

			Uprush							Backwash					
x (mm)	t_{ba} (s)	t_r (s)	t_L (s)	m_1 (g)	m_2 (g)	m_3 (g)	m_4 (g)	m_5 (g)	m_6 (g)	t_{dn} (s)	t_{up} (s)	m_1 (g)	m_2 (g)	m_3 (g)	m_4 (g)
CS: x = 0.062m															
602	2.303	4.788	2.525	1175	1146	1180	-	-	-	5.933	6.475	9	7	8	
			2.825	1918	1985	1927	1996	-	-	6.45	6.99	14	14	-	
			3.225	2024	2012	2205	2103	-	-	6.983	7.463	163	131	148	
			3.825	2309	1975	2144	2266	-	-	7.485	8.068	498	440	454	478
			4.788	2550	2465	2270	2161	2293	2321	7.971	8.549	381	393	340	402
CS: x = 1.447m															
1447	2.625	4.997	2.841	956	812	777	858	-	-	6.025	6.472	13	13	17	-
			3.141	1599	1844	1567	1712	-	-	6.536	7.128	279	228	212	-
			3.541	1944	1931	2055	2194	-	-	7.038	7.580	339	333	-	-
			4.041	2067	2014	2034	2104	-	-	7.525	8.107	245	251	212	-
			4.997	1949	2021	2016	2083	-	-	8.000	8.622	65	67	70	-
CS: x = 2.286m															
2286	3.053	5.194	3.343	770	917	777	881	-	-	5.529	6.084	12	13	14	-
			3.543	1147	1151	1123	1137	-	-	6.047	6.632	26	5	14	-
			3.743	1277	1298	1370	1373	-	-	6.565	7.148	68	95	-	-
			4.143	1309	1417	1392	1378	-	-	7.049	7.773	104	95	93	-
			5.194	1373	1452	1457	1451	-	-	7.535	8.349	4	2	3	-
CS: x = 3.117m															
3117	3.613	5.411	3.831	450	470	478	395	-	-	5.445	5.918	5	3	4	-
			4.031	632	675	664	670	-	-	5.849	6.312	3	1	6	-
			4.231	771	676	797	722	-	-	6.265	6.785	16	6	8	-
			4.631	829	794	776	760	-	-	-	-	-	-	-	-
			5.411	747	830	742	713	-	-	-	-	-	-	-	-
GV: x = 0.062m															
602	2.325	4.817	2.400	711	751	680	-	-	-	Backwash transport ~ zero					
			2.700	2138	2254	2154	2254	-	-						
			3.100	2712	2717	2567	2536	-	-						
			3.700	2740	2612	2710	2454	-	-						
			4.817	2711	2475	2820	2551	-	-						
GV: x = 1.447m															
1447	2.749	5.093	3.000	1749	1746	1665	1700	-	-	Backwash transport ~ zero					
			3.300	2892	2862	2984	2845	-	-						
			3.700	3279	3111	3326	3247	-	-						
			4.300	3319	3436	3467	3382	-	-						
			5.093	3473	3378	3522	-	-	-						
GV: x = 2.286m															
2286	3.468	5.324	5.324	1170	1291	1417	1238	-	-	Backwash transport ~ zero					

Table 1. Sediment flux measurements: trap timings and measured masses of collected sediment. t_{ba} = time of bore arrival; t_r = time of flow reversal, uprush to backwash; t_L = time at which uprush trap is lifted; t_{dn} = time at which backwash trap is lowered to the beach face; t_{up} = time at which backwash trap is lifted.

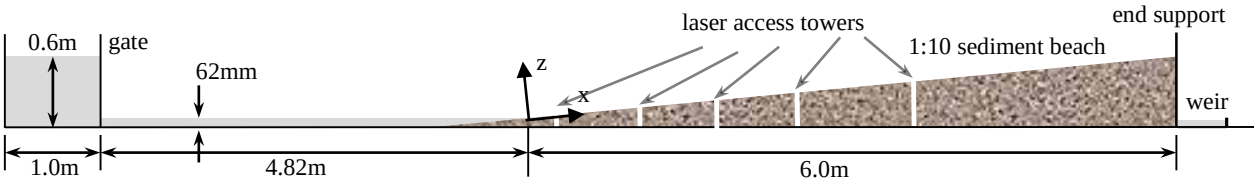

Figure 1: Schematic of experimental setup

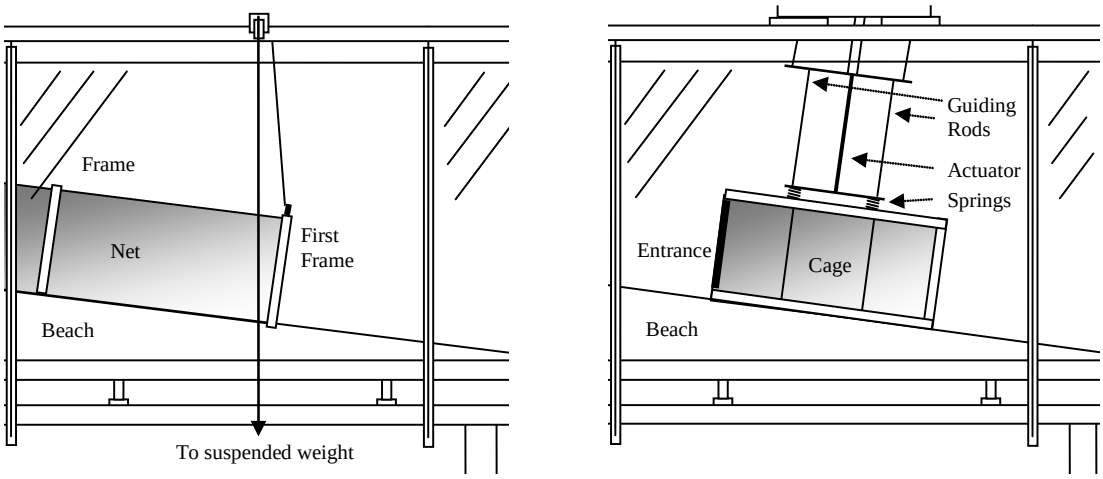

Figure 2: Schematic of uprush sediment trap (left) and backwash sediment trap (right)

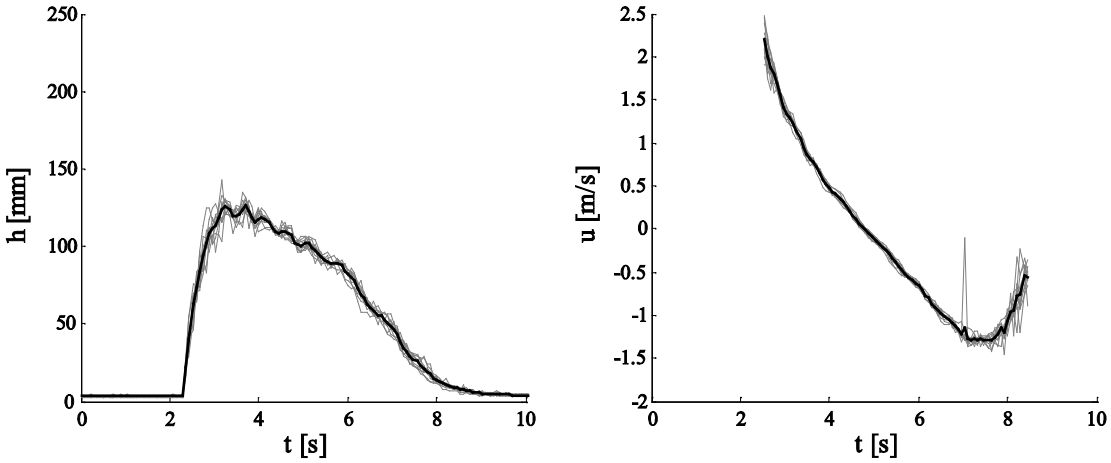

Figure 3: Example measured depth and depth-averaged velocity time-series (CS beach, $x = 0.772\mathrm{m}$); grey lines: 10 individual swash events; black line: ensemble-averaged result.

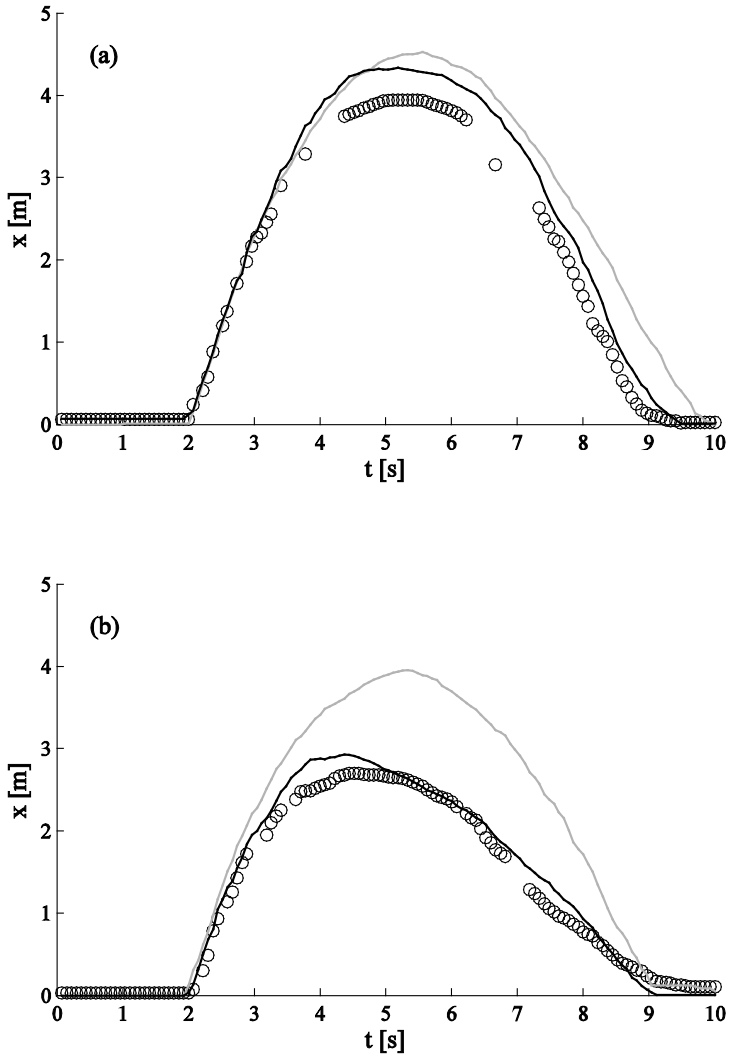

Figure 4: Shoreline position for (a) CS and (b) GV beaches. Circles: mobile beach, present experiments; corresponding results from Kikkert et al. (2012, 2013) for impermeable beach (grey line) and permeable beach (black line) are also shown.

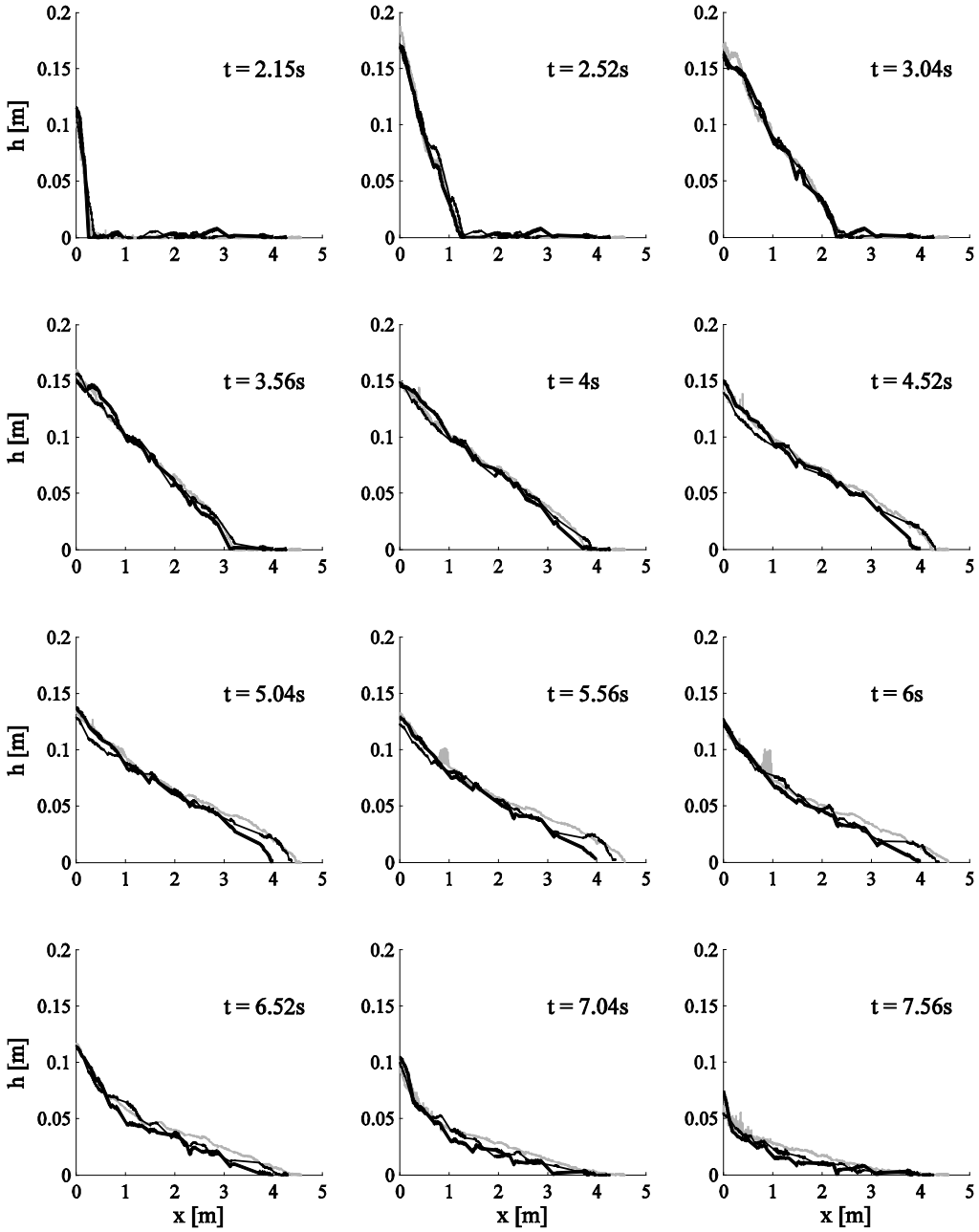

Figure 5: Swash lenses at 12 intra-swash times for the mobile CS beach (thick black line); corresponding results from Kikkert et al. (2012, 2013) for impermeable beach (grey line) and permeable beach (black line) are also shown.

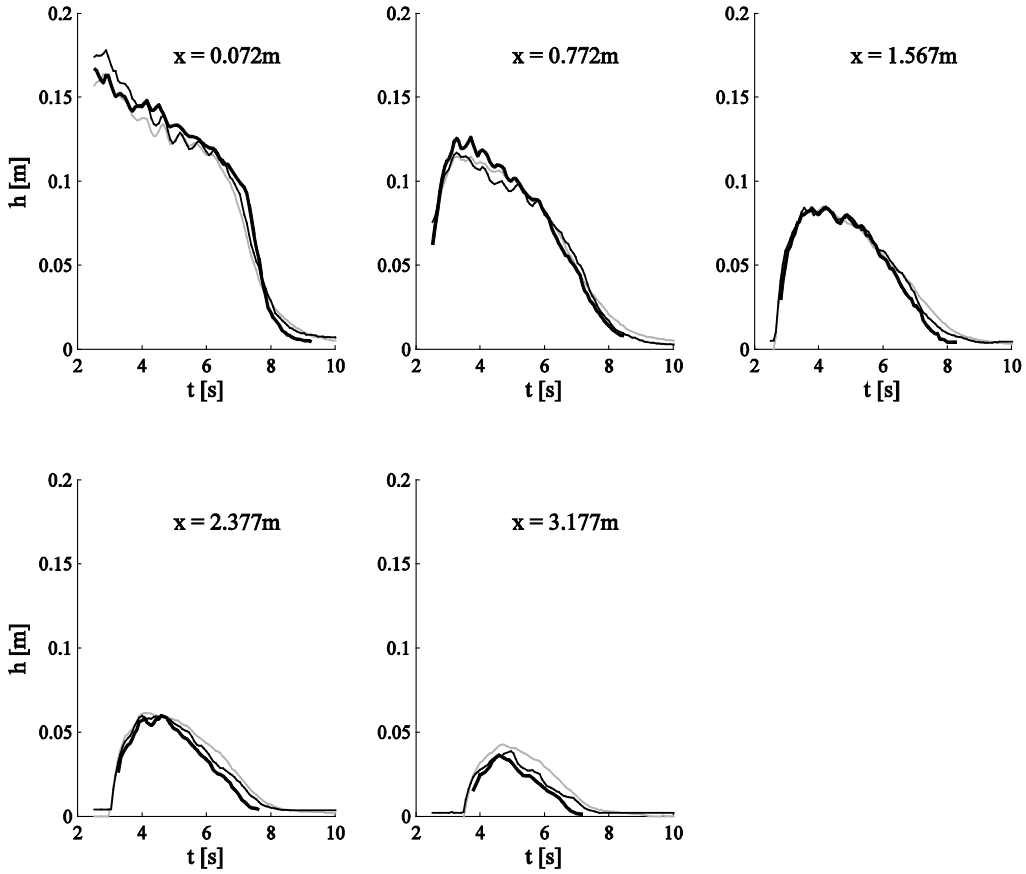

Figure 6: Depth time-series at 5 locations on the mobile CS beach (thick black line); corresponding results from Kikkert et al. (2012, 2013) for impermeable beach (grey line) and permeable beach (black line) are also shown.

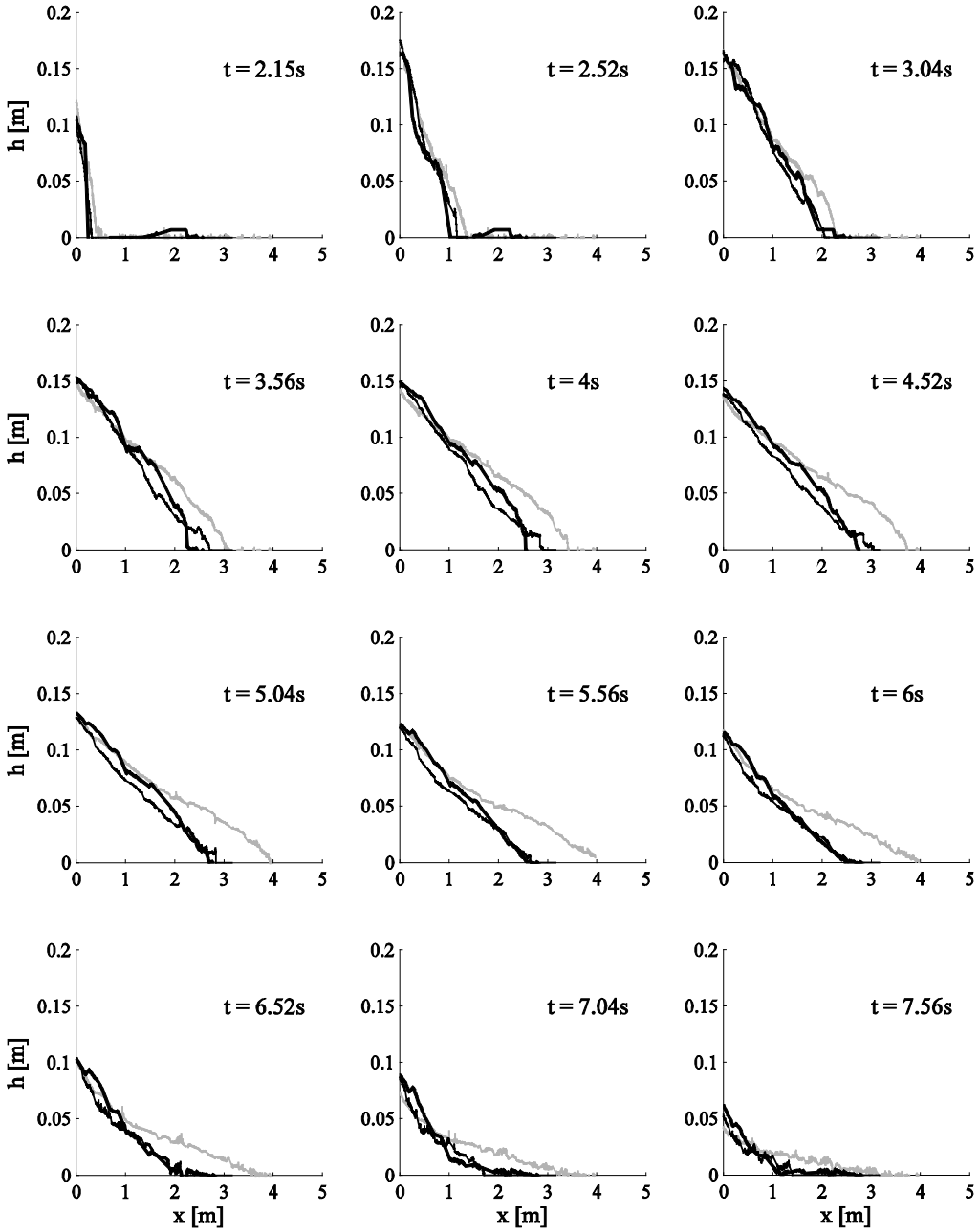

Figure 7: Swash lenses at 12 intra-swash times for the mobile GV beach (thick black line); corresponding results from Kikkert et al. (2012, 2013) for impermeable beach (grey line) and permeable beach (black line) are also shown.

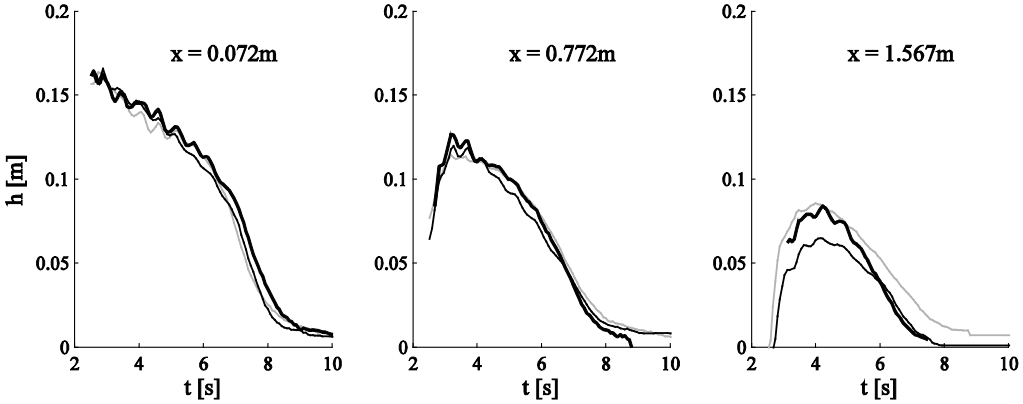

Figure 8: Depth time-series at 3 locations on the mobile GV beach (thick black line); corresponding results from Kikkert et al. (2012, 2013) for impermeable beach (grey line) and permeable beach (black line) are also shown.

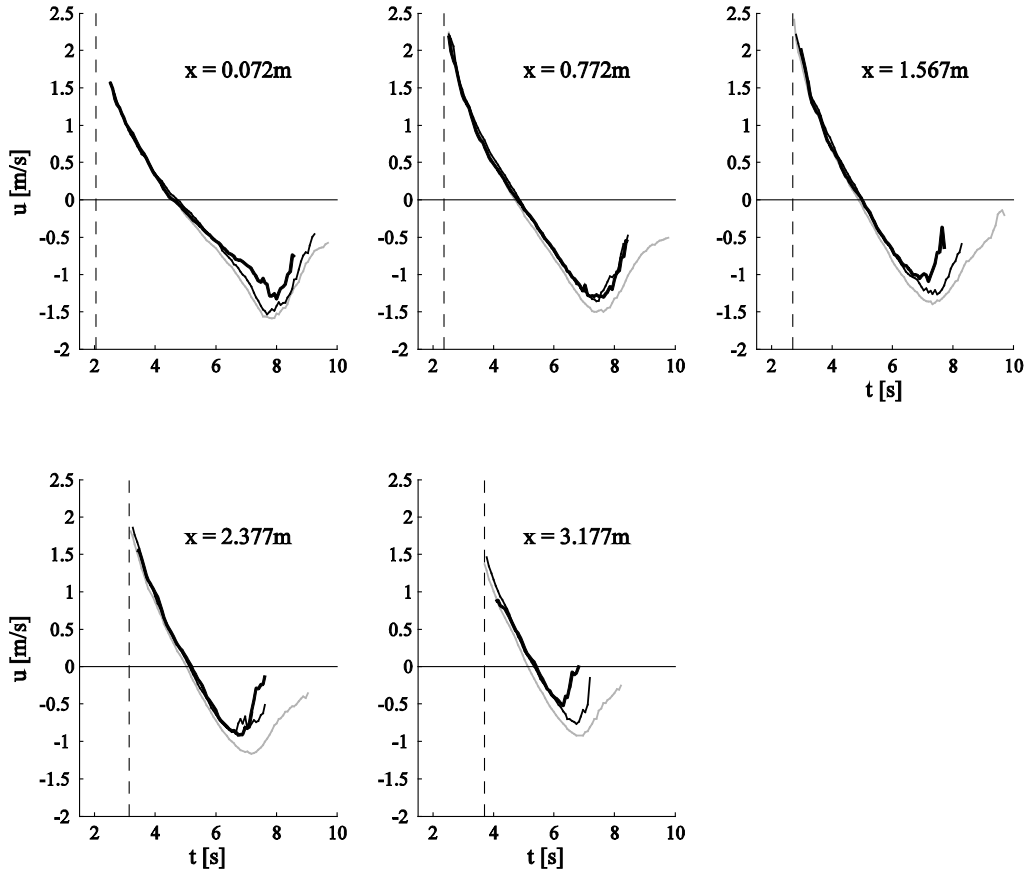

Figure 9: Time-series of depth-averaged bed-parallel velocity at 5 locations on the mobile CS beach (thick black line); corresponding results from Kikkert et al. (2012, 2013) for impermeable beach (grey line) and permeable beach (black line) are also shown; vertical dashed line indicates bore arrival time for the mobile beach.

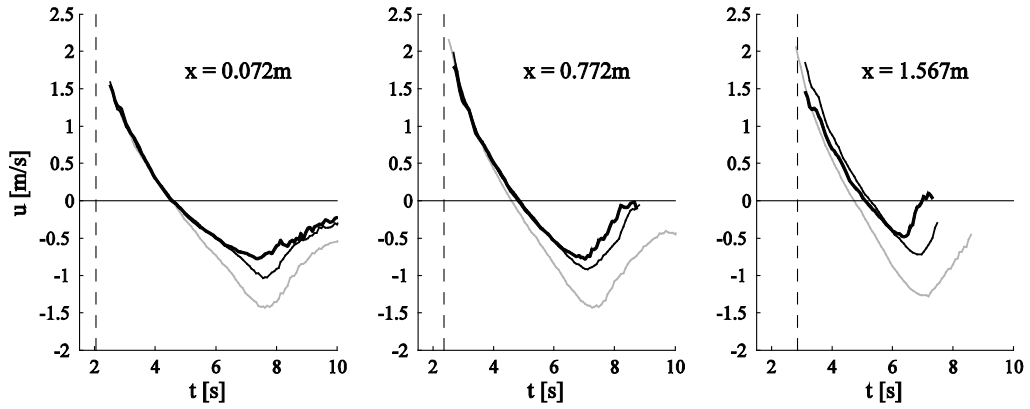

Figure 10: Time-series of depth-averaged bed-parallel velocity at 3 locations on the mobile GV beach (thick black line); corresponding results from Kikkert et al. (2012, 2013) for impermeable beach (grey line) and permeable beach (black line) are also shown; vertical dashed line indicates bore arrival time for the mobile beach.

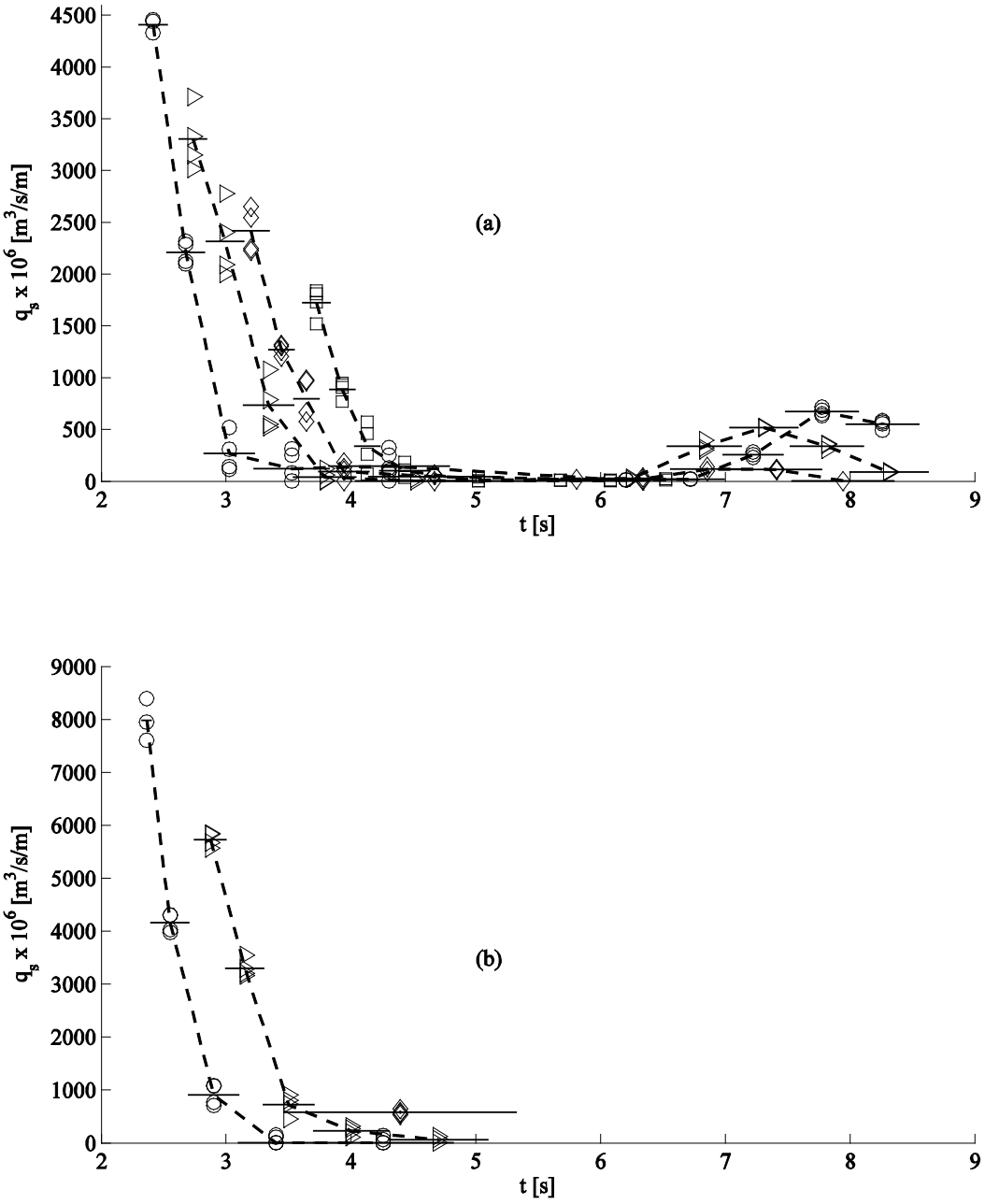

Figure 11: Measured intra-swash sediment flux for (a) the CS beach and (b) the GV beach; symbols correspond to x = 0.602m (circle), 1.447m (triangle), 2.286m (diamond) and 3.117 m (square); horizontal lines indicate average flux at each (x,t), with line length indicating trap duration; broken line joins average flux at each t for same x.

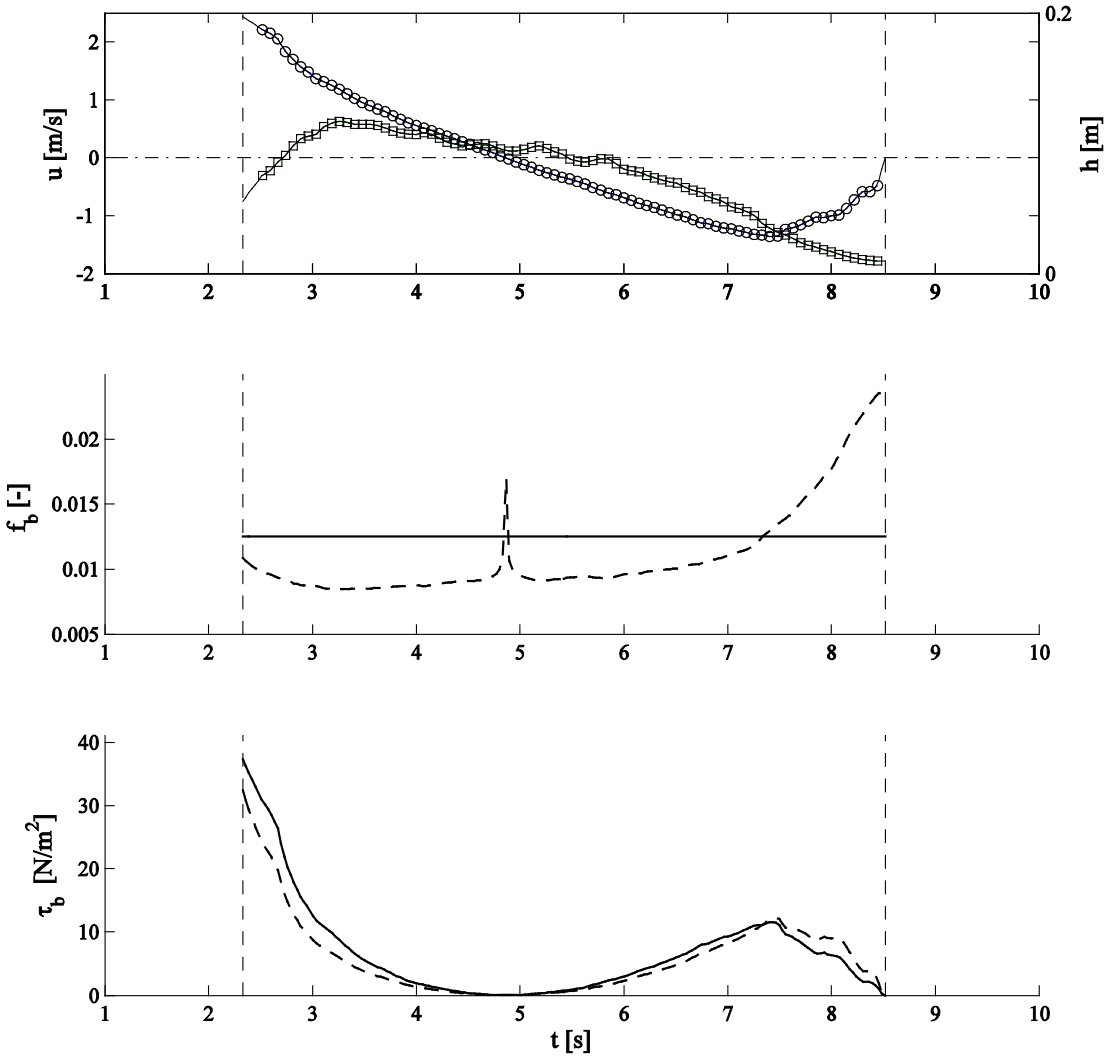

Figure 12: Example calculation of f_b and τ_b using Swart and Colebrook; input is $u(t)$, $h(t)$ measured at x = 0.772m on permeable coarse sand beach by Kikkert et al. (2013). Top: Measured $u(t)$ (circles) and measured $h(t)$ (squares); lines through the data are extrapolated and interpolated $u(t)$ and $h(t)$. Middle and bottom: f_b and τ_b respectively from Swart (solid line) and Colebrook (dashed line); vertical dashed lines correspond to $t = t_{ba}$ and $t = t_{end}$.

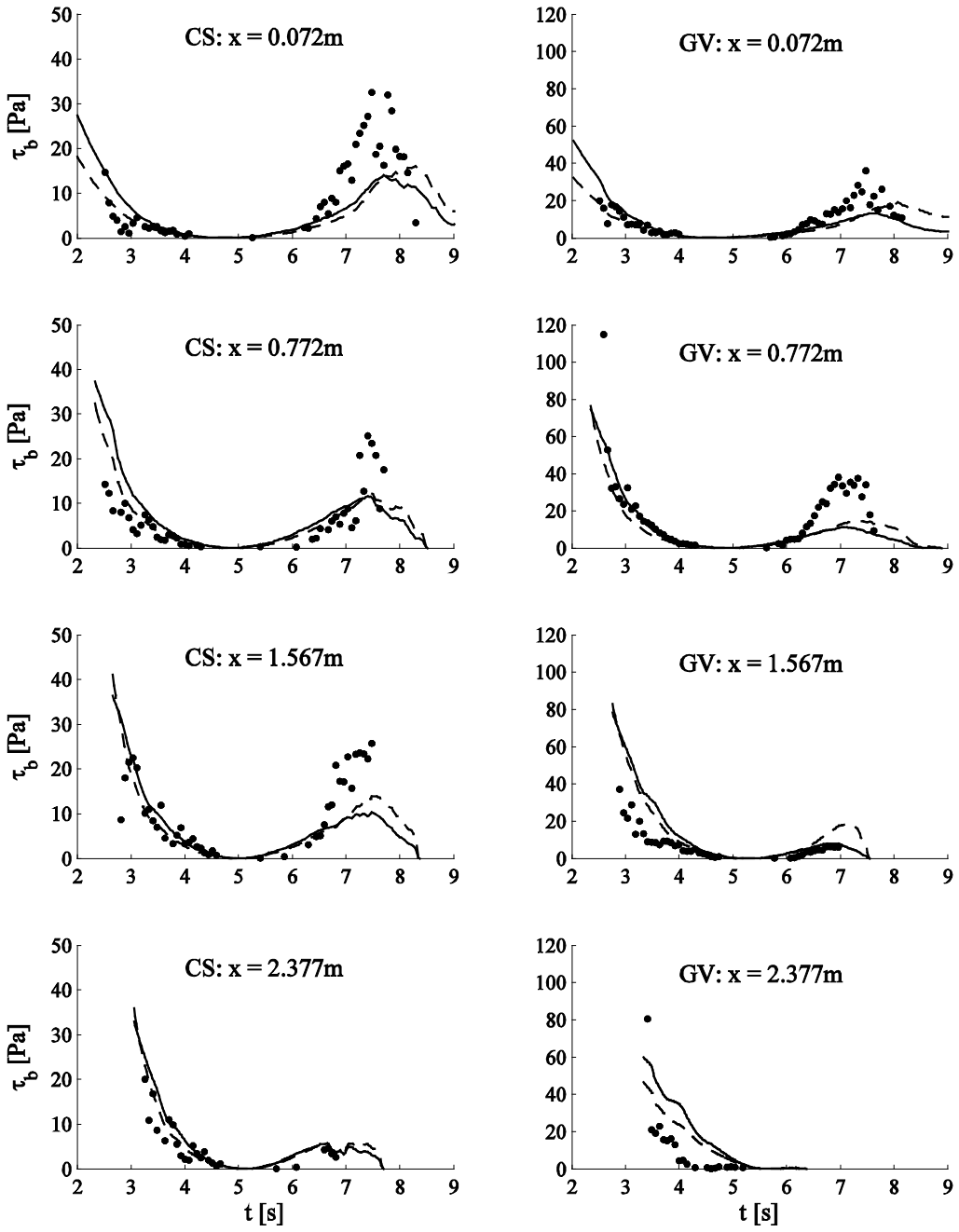

Figure 13: $\tau_b(t)$ calculated using Swart (solid line) and Colebrook (dashed line); input is $u(t)$, $h(t)$ measured by Kikkert et al. (2013) for swash on permeabe coarse sand (CS, left) and permeable gravel (GV, right) beaches; Kikkert et al.'s (2013) log-law-based $\tau_b(t)$ also shown (black dots).

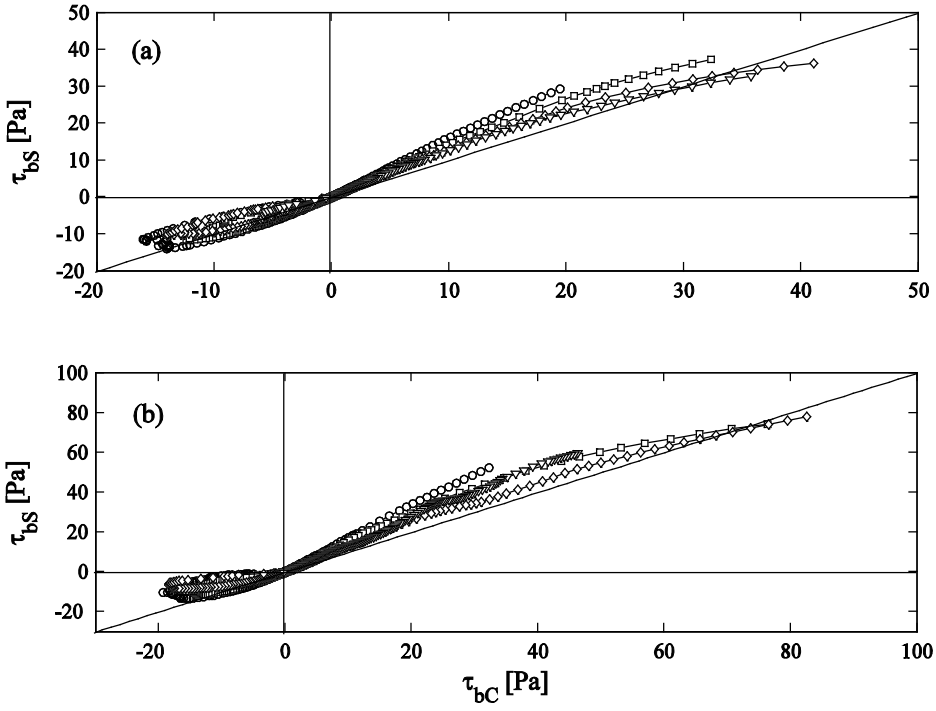

Figure 14: Swart bed shear stress (τ_{bS}) plotted against Colebrook bed shear stress (τ_{bC}) ; input is $u(t)$, $h(t)$ measured by Kikkert et al. (2013) for swash on (a) permeable coarse sand beach and (b) permeable gravel beach; measurements were made at 4 locations: x = 0.072m (circles), 0.772m (squares), 1.567m (diamonds) and 2.377m (triangles); diagonal line is line of perfect agreement.

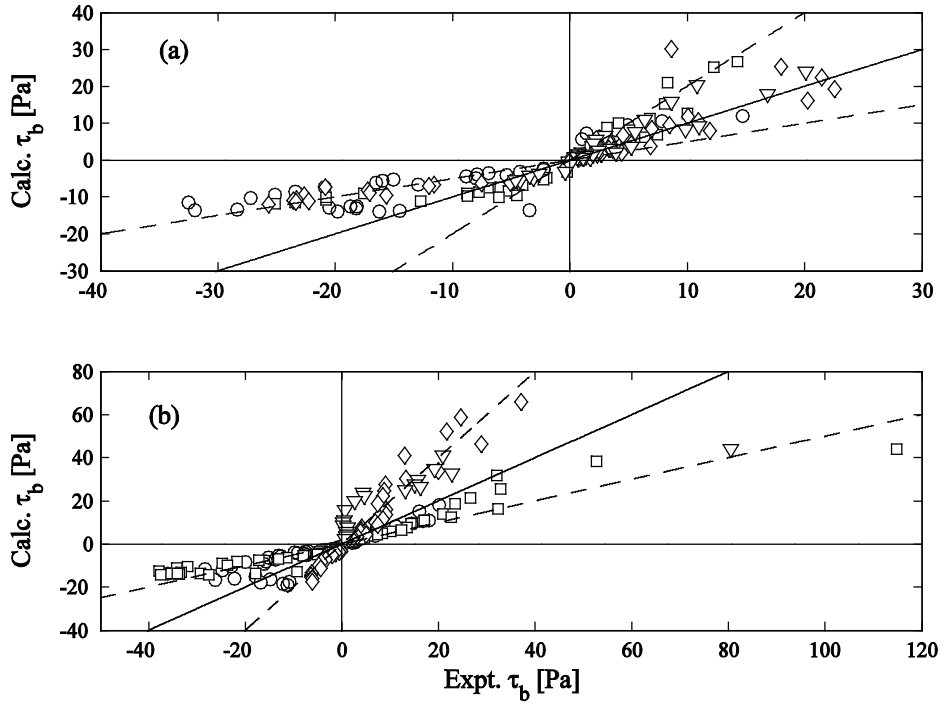

Figure 15: Calculated bed shear stress (mean of τ_{bS} and τ_{bC}) plotted against log-law-based experimental estimate of bed shear stress for Kikkert et al.'s (2013) (a) permeable coarse sand beach and (b) permeable gravel beach experiments; measurements made at 4 locations: x = 0.072m (circles), 0.772m (squares), 1.567m (diamonds) and 2.377m (triangles); solid line is line of perfect agreement and dashed lines indicate factor 2 difference.

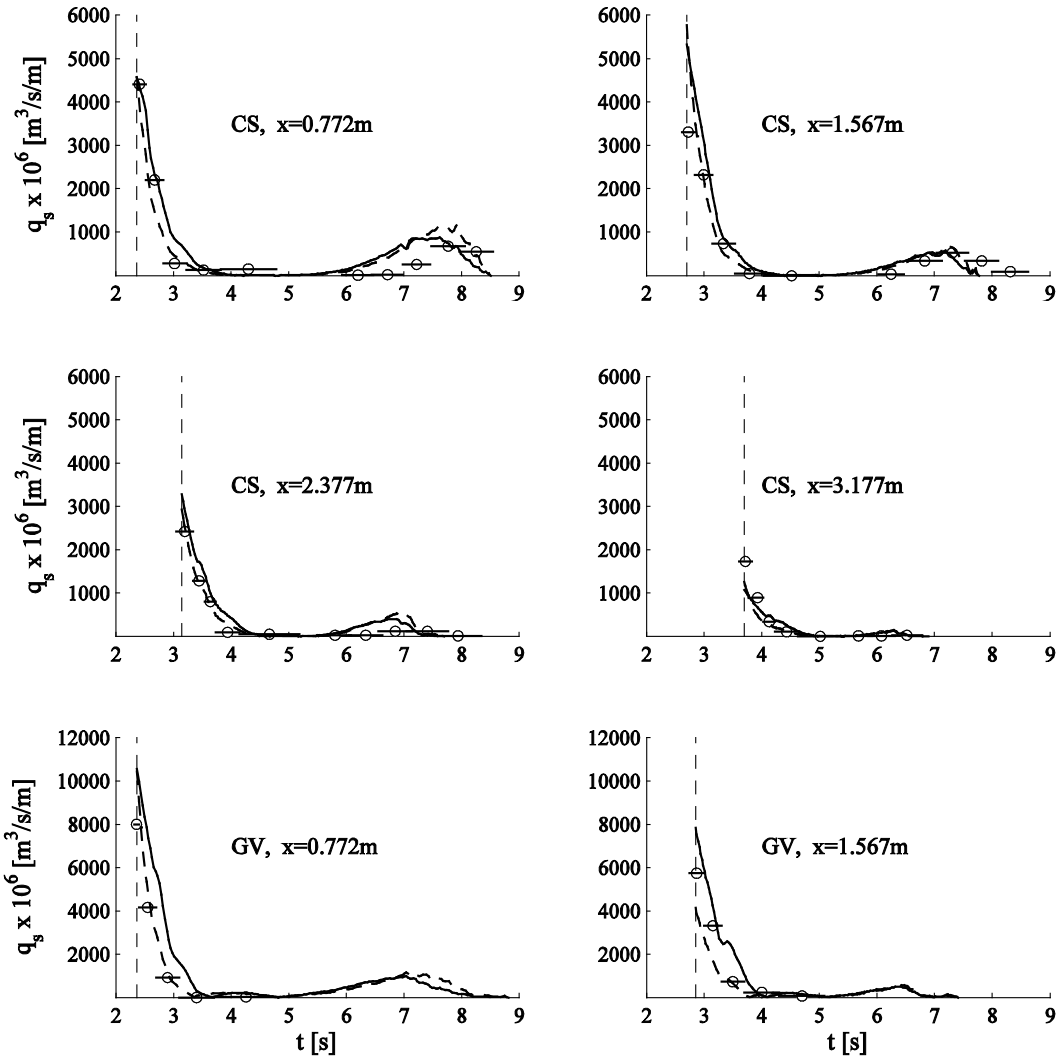

Figure 16: Measured and calculated intra-swash sediment flux at four locations on the CS beach (top four panels) and two locations on the GV beach (bottom two panels). Circles: averaged experimental results from Figure 11 with horizontal line indicating trapping duration; solid line: calculated flux using measured $u(t)$ as input and f_b calculated using Swart; dashed line: calculated flux using measured $u(t)$, $h(t)$ as input and f_b calculated using Colebrook; vertical broken line indicates time of bore arrival; note different vertical scales for CS and GV.

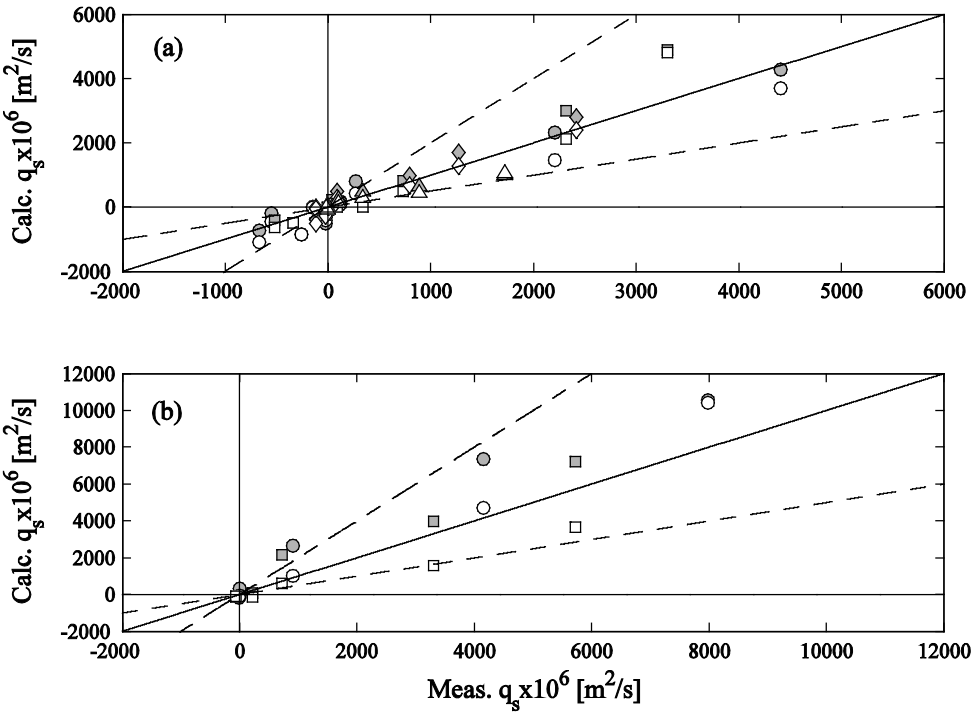

Figure 17: Calculated versus measured sediment flux for (a) the CS beach and (b) the GV beach; symbols correspond to x = 0.772m (circles), 1.567m (squares), 2.377m (diamonds) and 3.177m (triangles); solid and open symbols are results based on Swart and Colebrook respectively; solid line is line of perfect agreement and dashed lines indicate factor 2 difference.

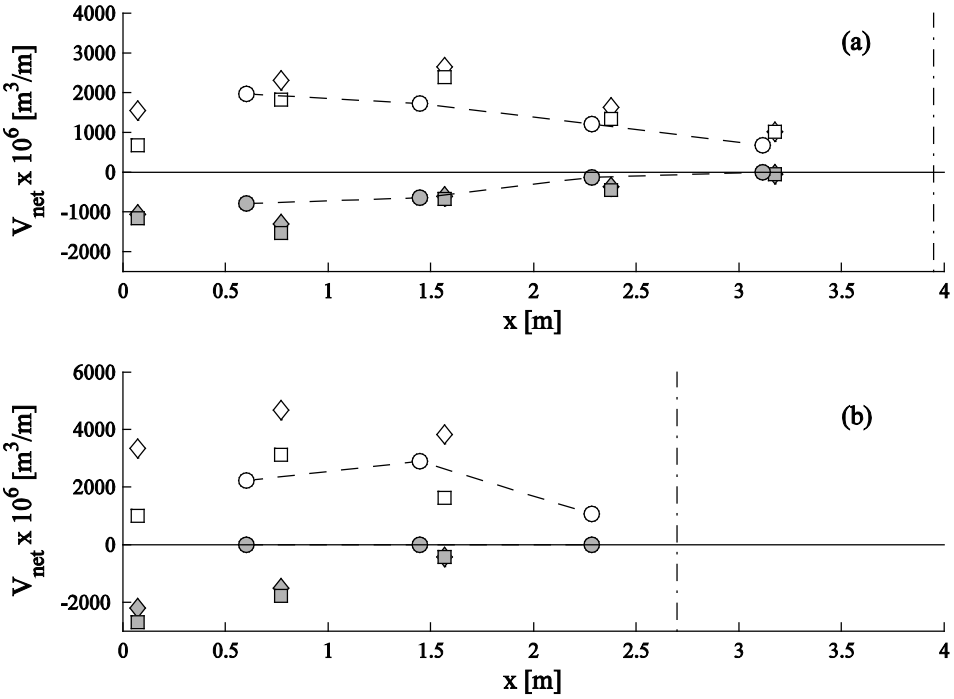

Figure 18: Measured (circles) and calculated (Swart: diamonds; Colebrook: squares) total uprush (open symbols) and total backwash (shaded symbols) sediment volumes transported on (a) the CS beach and (b) the GV beach; dashed line joins the measured values; vertical dash-dot line indicates location of maximum run-up.